MAGNETIC MATERIAL EFFECTS ON RF CIRCUITS

A THESIS
SUBMITTED TO THE FACULTY OF THE GRADUATE SCHOOL
OF THE UNIVERSITY OF MINNESOTA
BY

Alexander Patrick Nelson

IN PARTIAL FULFILLMENT OF THE REQUIREMENTS
FOR THE DEGREE OF
MASTER OF SCIENCE

Advisor: Rhonda R. Franklin

April 2018

Copyright page

Acknowledgements

I would like to thank Dr. Rhonda Franklin for her for her valuable technical advice and guidance. For the 4 years I have known her she has been a guiding light that has showed the RF world to me and taught me so much about it.

I would like to thank Dr. Bethany Stadler and Joseph Um for getting me started on the electromagnet measurements, and Wen Zhou for providing her code that chapter 3 is built on. I would also like to thank the members of my final exam committee, Dr. Anand Gopinath and Dr. Gregory Adriany for giving their time and energy to serve on my committee. I would also like to thank my fellow MPACT group members Chanjoon Lee, Wen Zhou, and Yali Zhang for assisting me by answering my questions and bringing me closer to understanding my problems.

Many friends, such as Steven Breuer, Max Utterberg, and Garrett Peloquin, assisted and encouraged me along the way, and without their help and encouragement I would not have completed my degree. I would also like to thank my sister who I love. I am forever grateful to my parents, Arlin and Maria, my grandparents Gerald and Beverly Falbo and Janet and Frank Nelson for supporting me and shaping me into the person I am today.

This thesis is dedicated to

Arlin, Maria, Katie, Frank, Janet Nelson and Gerald and Beverly Falbo

Abstract

This thesis discusses the interaction of magnetic materials and high frequency signals inside of microstrip transmission line circuits. This work is based on microstrip circuit designs that use magnetic materials for either the ground plane and/or as an insert inside the microstrip substrate. The microstrip circuits with inserts are characterized with AC and DC magnetic fields. The magnetic materials are bulk metals. The magnetic materials inserted into the circuit change how the circuit reacts to DC magnetic fields. When a DC magnetic field is applied the transmission of the magnetic materials shifts at each frequency.

Table of Contents

List of Tables

List of Figures

Chapter 1

Introduction

1.1 Motivation

With the advancement of communication technology, Radio Frequency (RF) and microwave circuits have become much smaller and more complicated and use many different materials, including magnetic materials. Magnetic materials can be affected by DC magnetic fields that originate outside of the circuit, and thus can change the circuit response. Because of the extreme magnetic with the frequency of the circuits with this materials may experience higher loss increase, due to excitation of the ferromagnetic resonance (FMR) [1-4] property of the magnetic material. Examples of circuits designed with FMR include filters ([5-7]), noise suppressors [8], and circulators [9-12]. FMR has been studied on a variety of RF structures including microstrip ([7], [13], [14]), stripline ([15-16]), and coplanar waveguide (CPW) ([17-19]). It has also being studied in various materials including thin films ([17], [20]), multilayer films ([16], [21]) and nanowires ([2], [7], [13], [14], [22], [23], [24]). In order to better understand the interactions between fields and embedded layers and bulk magnetic materials, microstrip transmission lines have been tested with bulk inserts between the signal line and ground plane compared to similar inserts with non-magnetic materials.

This thesis describes a physical microstrip circuit designed to characterize the response of bulk magnetic materials to AC and DC magnetic fields. Nickel is chosen as

the magnetic material characterized in this work because the change in nickel's permeability at the FMR point with applied magnetic field is well documented and understood ([1], [3]). A microstrip test structure is chosen for the direction of its internal fields as well as the ease of manufacture. Nickel is integrated into the microstrip circuit to characterize how magnetic materials carry RF signals.

1.2 Design Overview

There are 3 main chapters in this thesis. The characterization of magnetic materials when substituted for the ground plane of microstrip lines and also when materials are inserted into the microstrip lines is discussed in Chapter 2. Chapter 3 investigates the changes in circuit response when strong DC magnetic fields are applied to circuits with inserts inside them. A summary of this thesis and future directions for building on this work are provided at Chapter 4. Appendixes are provided for expanded computer simulations and for low DC magnetic field measurements that don't saturate the magnetic materials.

Chapter 2

Magnetic Material Characterization of Microstrip Circuits

2.1 Introduction

Microstrip transmission lines are popular in planar and integrated RF communication circuits. Their electrical properties depend on the dielectric (i.e. permittivity) and the metal (i.e. conductivity) layers of the substrate material. Microstrip lines have been used to test nanowires with the microstrip deposited onto of a substrate with nanowires grown in it ([7], [9], [13], [14], [23]) and thin films planted on top of the microstrip ([25]). The circuit designed in this chapter place a magnetic sample for FMR measurement between the substrate and ground plane. In this chapter, the performance of microstrip transmission lines is studied with metal inserts and different metal ground planes without a DC magnetic field.

The behavior of microstrip transmission lines is evaluated and characterized based on copper (non-magnetic) or nickel (magnetic materials) metals. The signal line is copper in all cases. Nonmagnetic materials have a relative permeability of 1 whereas the magnetic material, in this work nickel, has a relative permeability that is at least 100. Metal behavior impacts circuit resistance, inductance, impedance, and skin depth.

The objectives of this chapter are to study and characterize bulk magnetic metal effects on microstrip transmission lines. Bulk materials are chosen to establish performance a comparison for similar materials in thin films [15] or nonmagnetic [25]

form. The first objective is to understand the impact of bulk magnetic material on losses in microstrip. The second objective is to observe the behavior of insert metals underneath the feedline. The third objective is to understand how the insert metal type, nonmagnetic or magnetic, affects microstrip performance. These results establish a baseline for use of magnetic materials in RF/microwave circuit design.

2.2   Ground Plane Material Effects on Microstrip Lines

Microstrip transmission line fields, shown in Fig. 2.1, have electric fields (**E**, solid) that travel from between the signal line to the ground plane in the substrate while the magnetic fields (**H**, dashed) orbit the signal line. The electric fields define the voltage on the microstrip while the magnetic fields define the current. To absorb power from the system an absorber needs to be exposed to the **E** and **H** field. Eqn 1 describes the Poynting vector [27], a calculation of power (**S**) imparted by **E** and **H** fields via the cross product of their two fields. Power can be absorbed by placing an insert above the microstrip, between the ground plane and the microstrip's signal line, or by replacing the ground plane. Placing an insert above the microstrip will not interfere with the electric field so it will not be considered for repeatable measurements. In this chapter designs will be presented to measure both adding inserts and changing ground plane and the methods of measuring these circuits will be presented.

Figure 2.1 The field distribution of a Microstrip Transmission line [27]
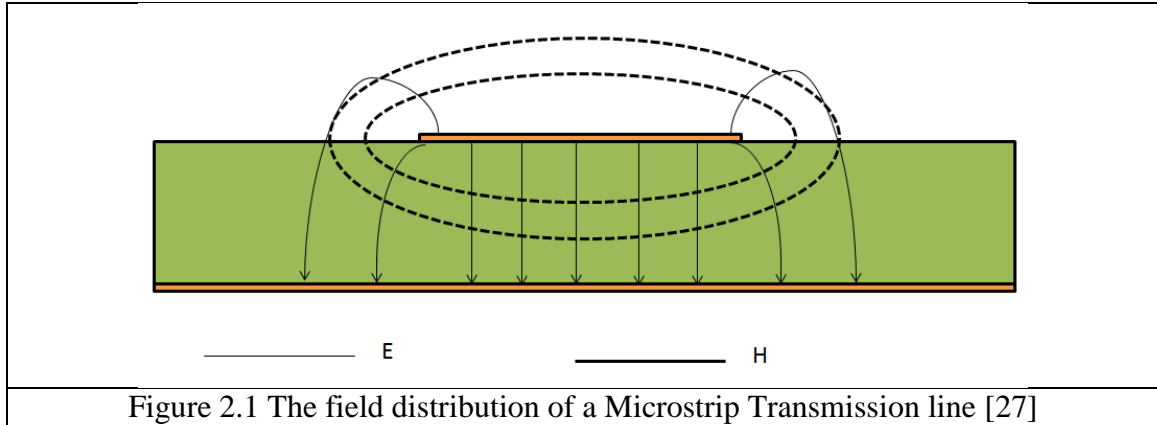
$$S = E \; X \; H \tag{1}$$

2.2.1 Design

Microstrip lines in this work, shown in Fig. 2.2, are designed using Linecalc and modeled in Advanced Design System (ADS) [28]. All designs are printed on a FR4 [29] fiberglass that serves as the dielectric substrate. The FR4 dielectric thickness (h) is 28 mils thick, relative permittivity (ε_r) is 4, and relative permeability (μ_R) is 1. The manufactured board material is double-sided copper with metal conductivity (σ) of 5.813×10^7 Siemens/meter [27] and metal thickness of 1.4 mils. These parameters are also shown in Table 2.1.

The reference line impedance is designed to be 50 ohms. In the study, the bottom copper layer (tc = 1.4 mils) is removed and replaced with either a copper foil (tg = 1.4 mils) or nickel shim (tg = 6 mils). To insulate the inserts from the ground plane, a thin (tp = 3 mils, ε_r=2) Melinex plastic [30] dielectric is included between the metal ground plane and FR4 board as seen in Fig. 2.2 and the signal line width is adjusted to maintain a 50

Ohm impedance. Nickel conductivity (σ) is 1.43 x 10^7 Siemens/meter [27] and relative permeability (μ_R) is 100 [31].

Figure 2.2 The microstrip transmission line and the Copper and Nickel ground plane where W is line width, tc is conductor thickness, h is dielectric thickness, tp is plastic thickness, and tg is ground plane thickness
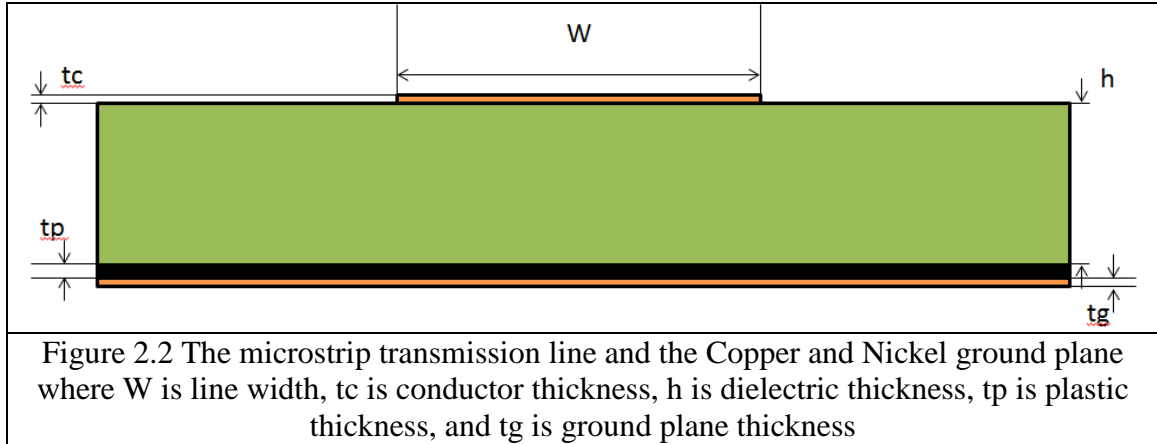
2.3   Simulation of Microstrip with Magnetic and Nonmagnetic Materials

Ideally circuit models like those used in Keysight's (ADS) and Linecalc would be used to predict circuit response (scattering parameters (S-Parameters) and characteristic impedance), but their simple models only work when all metal layers are the same material and the dielectric layers are of one type. This work considers circuits with mixed metals as well as double layer dielectrics (i.e. FR4, plastic) so these modeling tools cannot be used alone. Three dimensional full wave modeling software such as ANSYS's High Frequency Structure Simulator (HFSS) [32] and Quasi-static 3-D Extractor (Q3D) [33] are used to evaluate these cases. ADS and HFSS will be evaluated to determine their capability to simulate the reflection and transmission data of circuits used in this work while Q3D will be evaluated to determine their capability to simulate impedance.

2.3.1 Modeling Tool Introduction

The line discussed in chapter 2.2.1 will be modeled using several simulation tools (i.e. ADS, HFSS and Q3D). These tools differ in whether they model the physical geometries of the transmission lines or if they use predefined mathematical models. HFSS and Q3D are tools that replicate the physical structure of the circuit and use that structure to determine how the circuit responds to external sources. ADS reduces transmission lines to mathematical models based on their parameters (height, width, etc.) and computes the circuit response based on those models. Both simulation types will be tested to characterize their capability to replicate the measured circuits in this work.

An ADS circuit model, shown in Fig. 2.3, uses the parameters shown in Table 2.1 to replicate the fabricated microstrip line. The parameters of the FR4 substrate used in this simulation match the FR4 dielectric (Isola 185 HR [29]) that will be used for measurements with fabricated circuits. The coaxial lines on both sides of the microstrip line are part of the UTF [34] shown in Fig. 2.10 (the UTF will be described in chapter 2.3.3) that cannot be calibrated out of the measurements. Impedance is predicted with Linecalc to be 50 Ohms. Linecalc is useful only for designing the initial circuit and will not be used for anything else in this work. ADS assumes an infinite ground plane. Both signal line and ground plane are copper. Neither ADS nor Linecalc include the Melinex plastic layer between the ground plane and FR4 material. The ADS simulation is set up to simulate from 40 MHz to 20 GHz with 401 equally spaced points in between.

Table 2.1 Microstrip substrate parameters

Material Type	Parameter	Value
FR 4	Dielectric Constant (Er)	4 (unitless)
	Thickness	28 mils
	*Loss tangent (TanD)	0.02 (unitless)
Plastic (Melinex)	Dielectric Constant	2.8 (unitless)
	Thickness	2 mils
Copper	Thickness	1.4 mils
	Conductivity	5.813×10^7 (Siemens/meter)
Nickel	Thickness	3 mils (insert), 6 mils (ground)
	Conductivity	1.43×10^7 (Siemens/meter)
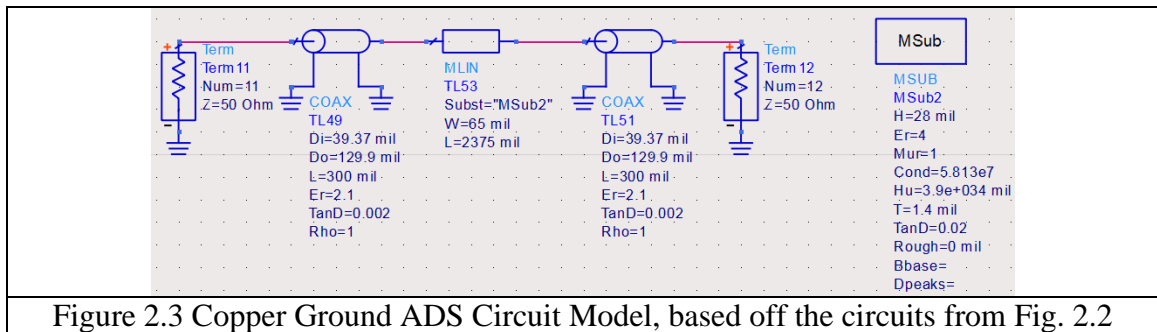
Figure 2.3 Copper Ground ADS Circuit Model, based off the circuits from Fig. 2.2

ADS's simple mathematical model only allows for 1 homogenous dielectric substrate, but later on in this work the dielectric substrate will be composed of multiple dielectric layers that ADS will be incapable of modeling with its simple structures. ADS also assumes that the signal line and ground plane will be made of the same metal material, so when the nickel ground is simulated ADS also defines a Nickel signal line.

To account for mixed metal materials and the plastic layer between FR4 and ground planes Q3D and HFSS are used. Q3D is used to determine the impedance of the microstrip structure while HFSS computes S parameter data that describes reflection and transmission. Q3D and HFSS are capable of independently defining the signal line and

8

ground plane while also defining multiple dielectric layers. The circuit geometry used in Q3D and HFSS will match the circuit used in the ADS simulations.

Q3D is a full wave modeling tool that computes the lumped element values for R, L, G, and C of the input design. The cross section of a structure is shown in Fig. 2.4. Q3D models physical circuits and therefore cannot accept an infinite group plane, so a substrate width of 1570 mils (4 cm) is chosen for the simulation and eventually the fabricated circuit. The two structures that are modeled are based off the ADS structure from Fig. 2.3 and using the values from Table 2.1. These models have a plastic dielectric material inserted between the FR4 dielectric layer and the ground plane. Once Q3D has calculated the model's R, L, G, and C parameters they are exported as a touchtone .s2P file that can be read into ADS or other analysis software. Eqn 2 [27] describes the calculation of characteristic impedance of the microstrip lines with the R, L, G, and C parameters calculated from Q3D. The two designs in this work, microstrip with nickel ground and microstrip with copper ground, are homogenous in the length dimension and the impedance along the line length is a constant.

Figure 2.4 The cross section of the microstrip line used in Q3D to model the Copper Ground circuit measured in chapter 2.3.2
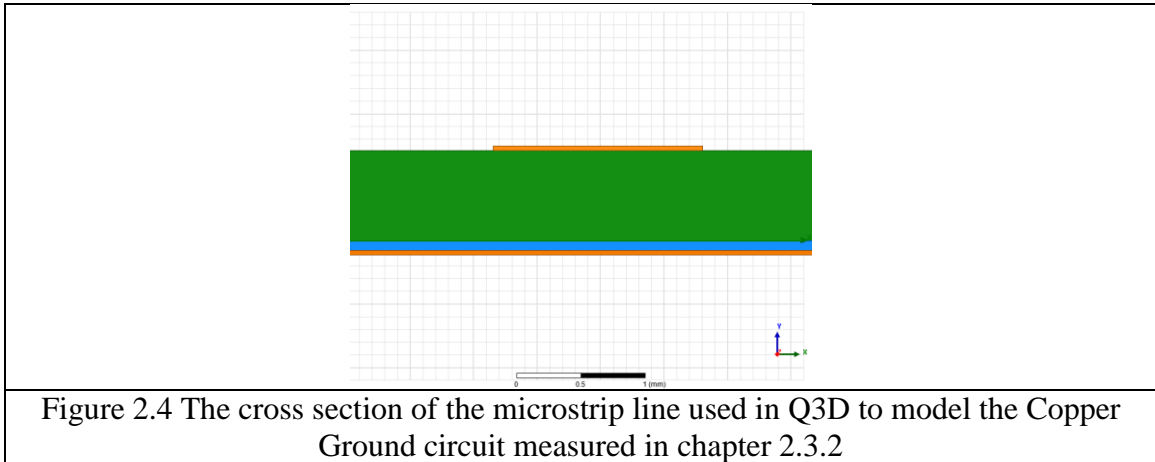
$$Z0 = \sqrt{\frac{R+j\omega L}{G+j\omega C}} \ Ohms \tag{2}$$

HFSS is a 3D simulation tool that computes S parameters based on complex electric and magnetic fields in a structure. This tool will allow inclusion of different metals and multiple dielectric layers. HFSS exports touchstone .s2P files that can be imported to other software and analyzed. The HFSS model, shown in Fig. 2.5, uses the dimensions defined in Table 2.2 and electrical parameters from Table 2.1. The HFSS model matches the cross section defined in the Q3D model so that the impedance remains constant between the two models. A wave port excitation is used and set to 50 Ohms on both ports. The simulation frequency range is 40 MHz to 20 GHz with 401 equally spaced data points. An air box is used on all models with the far field radiation boundary conditions applied to each non-magnetic face where only the ground plane with nickel poses an exception.

Figure 2.5 HFSS 3D model of Copper GND microstrip line with a copper signal line with dimensions based on Table 2.2
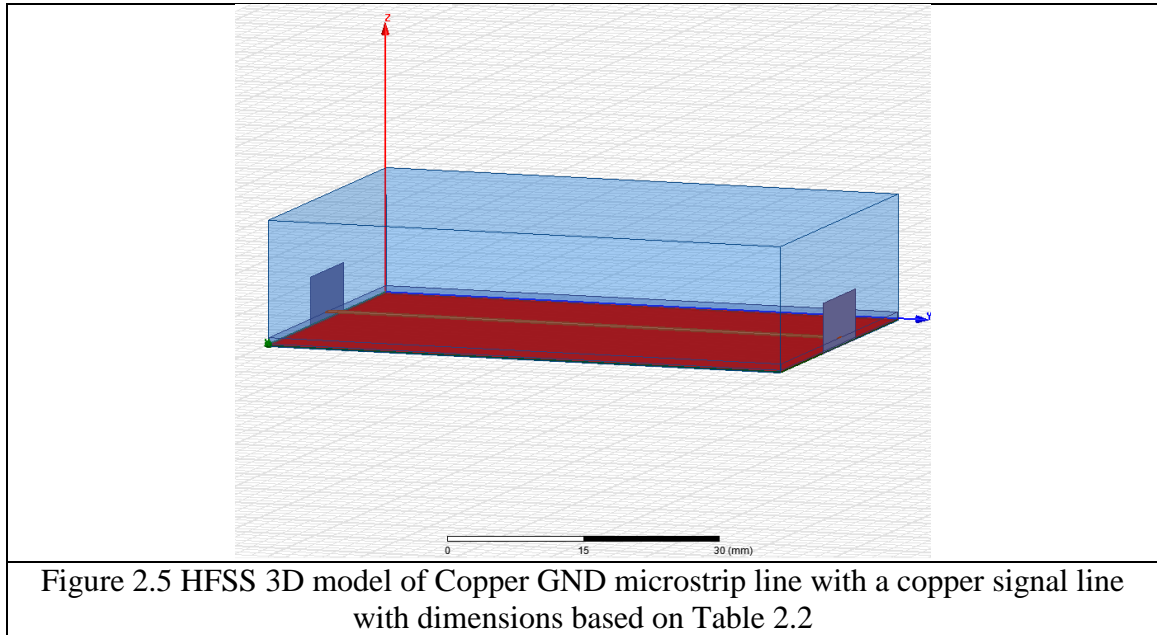
Table 2.2: Dimensions of HFSS simulations

Dimension	Value
Length	2375 mils
Substrate width	1573 mils
Line width	65 mils
Dielectric thickness	28 mils
Melinex thickness	3 mils
Conductor thickness	1.4 mils
Ground thickness	6 mils (nickel) or 1.4 mils (copper)

2.3.2 Q3D Impedance Simulation Results

The impedance data from Q3D is plotted in Origin [35] and shown in Fig. 2.6 for microstrip with different metal grounds and with plastic layer. Q3D calculates the characteristic impedance that varies over frequency, but it varies by about half an Ohm over the 20 GHz range. The copper ground simulation also has rising impedance over time while the nickel ground simulation remains constant. This is within 1 Ohm of the desired 50 Ohm characteristic impedance. The Q3D model matches the cross section of the HFSS model shown in Fig 2.5, so it follows that the HFSS model also has a characteristic impedance of roughly 50 Ohms.

Figure 2.6 Q3D impedance of microstrip with copper ground (black, dashed) and nickel ground (red, solid)
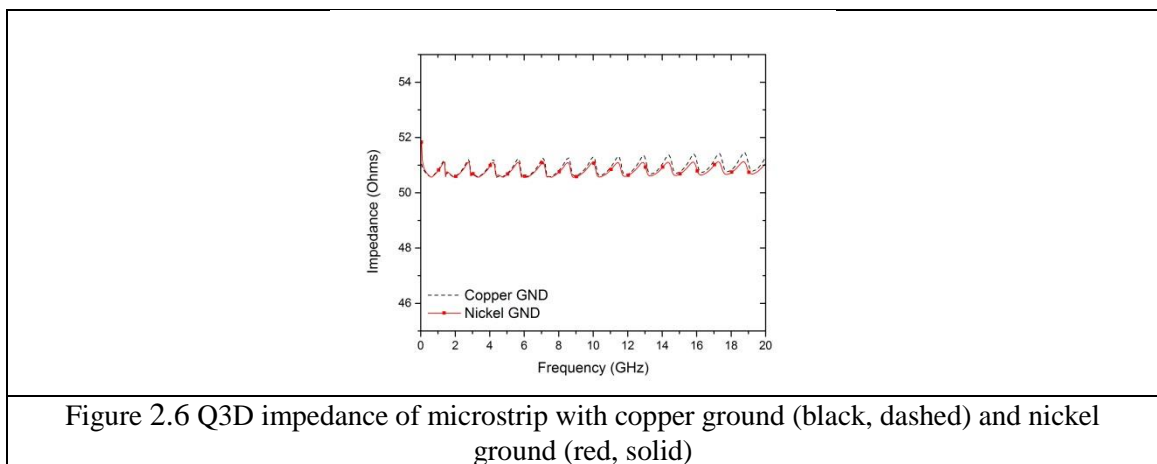
2.3.3 Model Comparisons

In Figs. 2.7 and 2.8 ADS and HFSS S parameter simulation results are compared with different ground planes. For both copper (Fig 2.7) and nickel (Fig 2.8) the reflection response (S11, (a)) and transmission response (S21, (b)) are shown. Reflection data (S11 or S22) is shown for the various test circuits to indicate mismatch between the VNA and the different circuits, and Transmission data (S21 or S12) indicates the performance loss due to the dielectric and conductors in the line. The ADS model is in solid red with squares, measured results are in dashed black, and the HFSS model is in blue with x symbols. The ADS model only allows for one metal the nickel ground measurement assumes the signal line is nickel as well.

Figure 2.7 The (a) reflection and (b) transmission response of the ADS model (red, square) and HFSS model (blue, x) with copper ground plane

Figure 2.8 The (a) reflection and (b) transmission response of the ADS model (red, square) and HFSS model (blue, x) with nickel ground plane
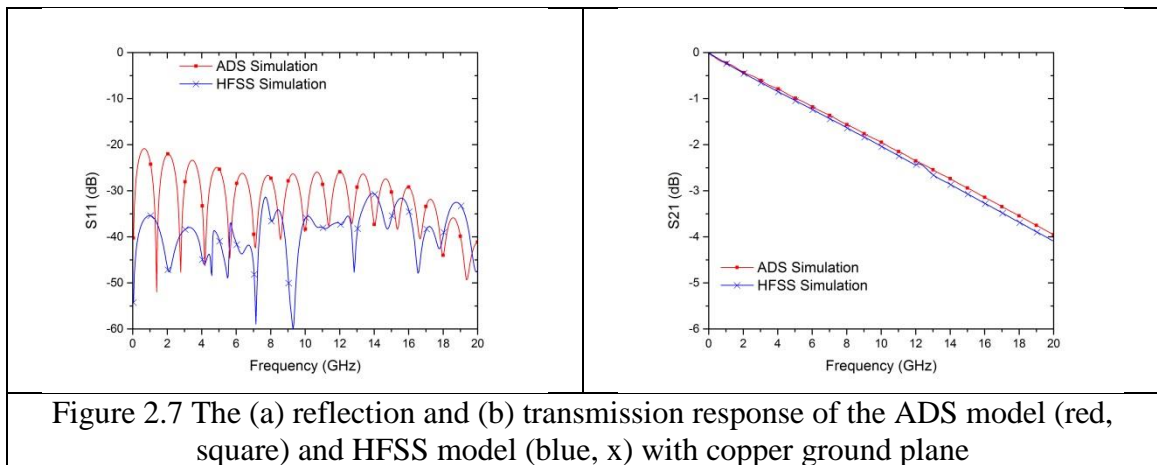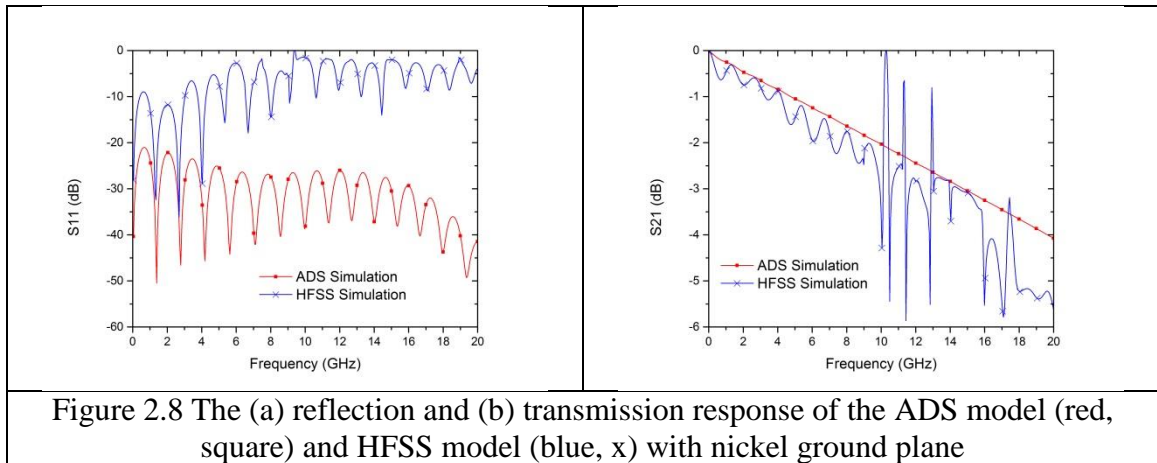
Fig. 2.7 shows the reflection coefficient and transmission response of the copper ground simulations and when the actual copper ground thickness and plastic parameters are included in the HFSS model. HFSS data is solid blue with x symbols, ADS data is solid red with circles and the measured results are in dashed black. The modeled results are less than -20 dB across the band for both ADS and HFSS. The connectors, included in ADS (but not in HFSS), account for phase shift but not mode transitions. The transmission of the ADS and HFSS models are similar with the copper having slightly higher transmission across the frequencies measured.

Fig. 2.8 compares ADS and HFSS simulations of reflection and transmission S-parameter data with a nickel ground plane. HFSS data is solid blue with x symbols, ADS data is solid red with circles. The models with a nickel ground plane use parameters from Table 2.1, except the HFSS model has a ground plane that is 3 mils thick (to allow the simulation to converge) and in ADS the signal line is also 6 mils thick and nickel (due to only being able to define 1 metal thickness). While the reflection data of the ADS

13

simulation are similar between copper and nickel ground, the HFSS simulation data are drastically different with HFSS predicting greater than -10 dB reflection with the Nickel ground indicating that the impedance of the circuit is mismatched from 50 Ohms. The transmission of the ADS simulation is similar to the copper ground, but the HFSS nickel ground transmission shows mismatch between 40 MHz and 10 GHz before the transmission data becomes unusable.

This chapter established that nickel ground and copper ground perform differently in simulation. Both copper ground simulations have a linear transmission response and a matched reflection, but HFSS cannot model the magnetic material when used as a ground plane. The HFSS model cannot accurately predict the impedance matching of the nickel ground plane. The ADS reflection and transmission data share a similar trend and together these are a theoretical baseline for measured results. In the next chapter, insert effects will be modeled.

2.3.4 Model Compared to Measurement

To determine the intrinsic properties of the circuit, physical circuits will be fabricated, measured and compared to the simulations. Transmission coefficient and reflection coefficient are measured as S-Parameters and will be used to compare the measurement against the simulation. The microstrip lines used in this work are fabricated on an LPKF Protomat S103 [36] and shown in Fig 2.9. The microstrip is fabricated with the signal line on an FR4 dielectric and then a sheet of Melinex and the ground plane (either copper or nickel) are placed on the bottom before the circuit is placed in the UTF.

Figure 2.9: Microstrip transmission line with copper and nickel ground plane

Measurements of microstrip lines are done with a Universal Test Fixture (Fig 2.10) or SMA connectors. The test fixture is used with no external B-field measurements and the VNA only and the SMA connector with external B-field measurements, discussed in chapter 3, and with the VNA. A 40 GHz Anritsu 37369D Lightning Vector Network Analyzer ([37]), shown in Fig. 2.11, is used with SOLT (Short-Open-Load-Thru) calibration [38] from 40 MHz to 20 GHz. The resolution of 49.8 MHz is based on 401 data points spread evenly across the frequency range. The SOLT calibration shifts the reference plane from the VNA to the input connectors of the UTF. A block diagram of the VNA measurement setup is shown in Appendix A. All measurement data is taken with WinCal [39] saved in .s2P format and includes the microstrip line plus input and output connectors of the UTF. The dimensions of the output connectors of the UTF are compared to the size of the microstrip lines in Appendix A.
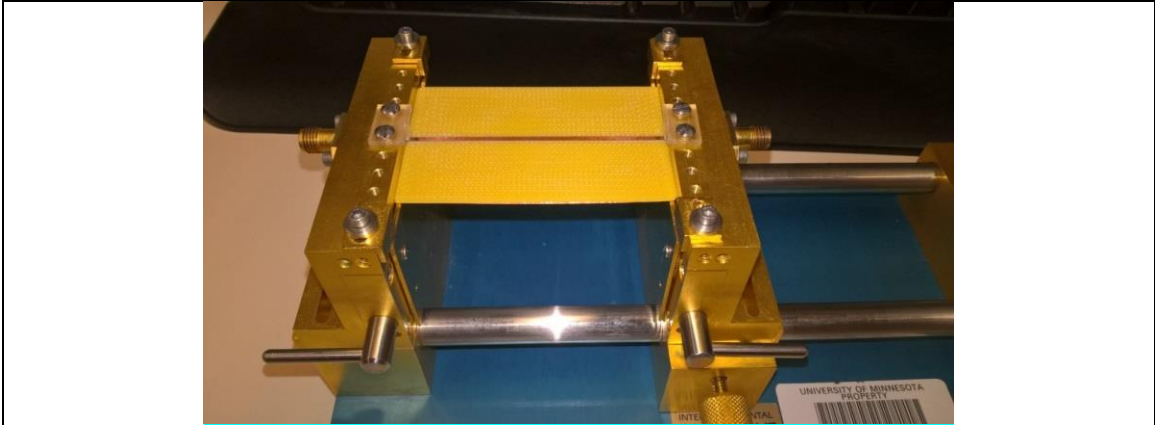
Figure 2.10 Universal Test Fixture

Figure 2.11 Anritsu 37369D Lightning VNA

Measurement results that compare the ground plane effects are described next. The reflection and transmission data shown in Figs. 2.12a and 2.12b represent the copper ground plane while the reflection and transmission data for the nickel ground plane are shown in Figs. 2.13a and 2.13b. The resulting loss calculation that comes from the VNA measurement is shown in Fig 2.13c for microstrip with the copper and nickel ground planes.

The reflection data of both designs are shown in Fig. 2.12a and Fig. 2.13a. Both have a reflection coefficient below -10dB above 3 GHz. The nickel reflection data are

slightly higher in the ranges of -5 to -8 dB. Both have resonance peaks below 3 GHz that

rise to -7 dB for copper and -10 dB for nickel. Fig. 2.12b and Fig. 2.13b show the

transmission response for copper and nickel ground planes respectively. Both lines have

similar transmission response across the band in the 3~14 GHz. Below 3 GHz, the copper

ground plane transmission is non-linear and it has more loss than nickel ground, and

above 14 GHz the nickel ground transmission drops far lower than the ADS simulation.

The copper transmission is better than the ADS simulation above 2 GHz and the nickel

transmission matches the ADS simulation up to 11 GHz before it drops below ADS's

linear result. Overall the transmission values from simulation predict a linear

approximation of the transmission of both the copper and nickel ground plane, but neither

HFSS nor ADS can predict the level of mismatch in the reflection coefficient.

Another useful metric is the total loss of the circuit and the copper and nickel

ground VNA measurements are shown in Fig. 2.13c. Fig. 2.13c shows the loss

calculation based on eqn 3 and plotted for both the copper and nickel ground planes. It is

notable that the loss in microstrip with nickel ground is less than the microstrip with

copper ground. Nickel is a more lossy metal than copper and therefore it should have

more loss than copper at all frequencies. To help determine where the differences

between the lines the dielectric loss (eqn 4), conductor loss (eqn 5), and surface resistance

(eqn 6) will be considered. The dielectric attenuation of the FR4 doesn't change between

the two lines, but the conductor loss changes based on the surface resistance. The surface

resistance is based on the conductivity of the material, and since the conductivity of

copper is 4 times larger than the conductivity of nickel the expectation is that the copper

ground should have lower loss. Since the dielectric attenuation is the same between the two and the conductor attenuation is higher for nickel the loss should also be higher, but in the measurement it isn't.

$$loss = 1 - |S11|^2 - |S21|^2 \tag{3}$$

$$\text{Attenuation, dielectric} = \frac{k0*\mathcal{E}r*(\mathcal{E}e-1)*\tan(\delta)}{2*(\mathcal{E}r-1)*\sqrt{\mathcal{E}e}} * \frac{1}{8.6859} \; dB/meter \tag{4}$$

$$\text{Attenuation, conductor} = \frac{Rs}{Z0*W} * \frac{1}{8.6859} \; dB/meter \tag{5}$$

$$Rs = \sqrt{\frac{2*\pi*f*\mu0}{2*\sigma}} \; Ohms \tag{6}$$

(a)   (b)
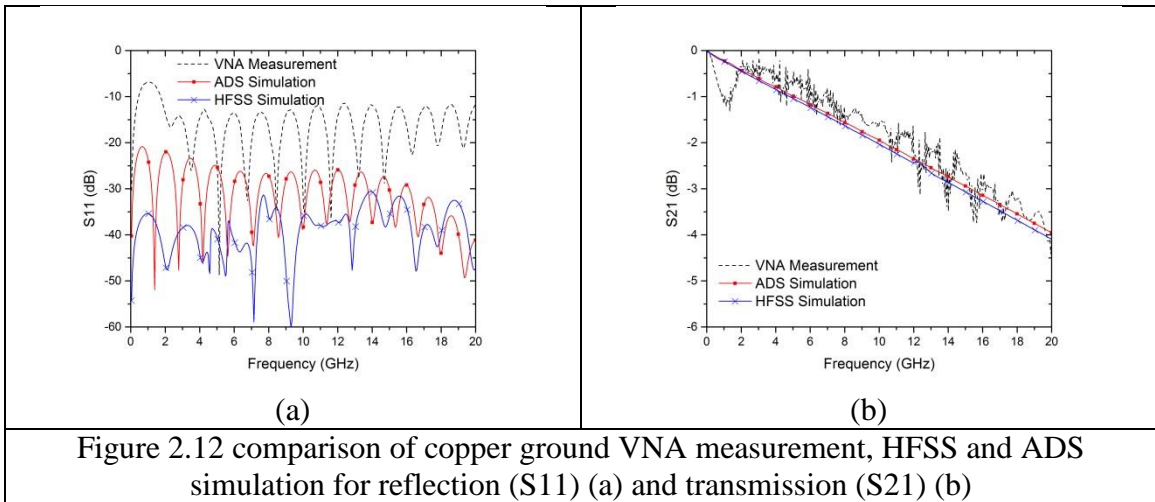
Figure 2.12 comparison of copper ground VNA measurement, HFSS and ADS simulation for reflection (S11) (a) and transmission (S21) (b)

(a)

(b)

(c)

Figure 2.13 reflection (S11) (a) and transmission (S21) (b) comparison of copper ground VNA measurement, HFSS and ADS simulation, (c) Copper vs Nickel ground plane loss calculation
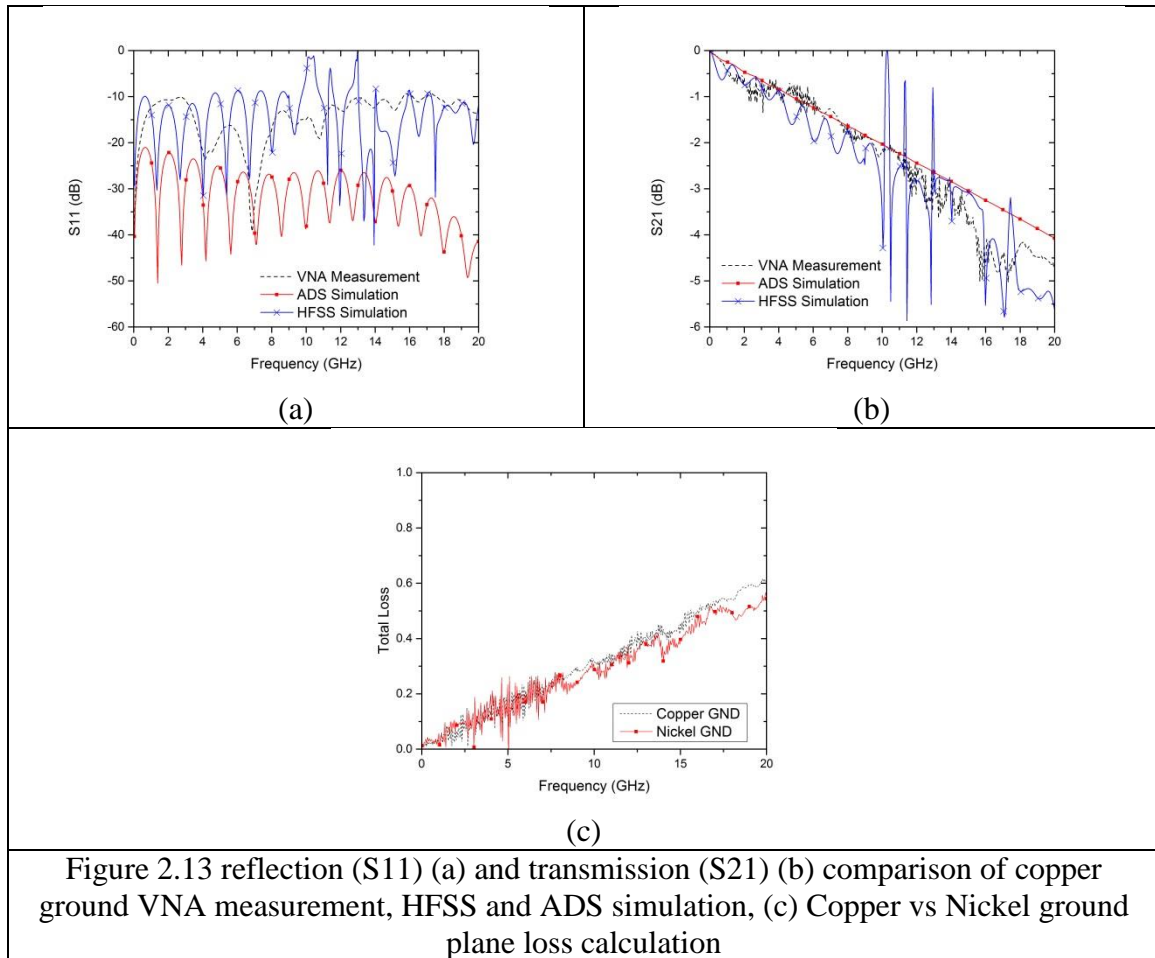
In summary, microstrip lines with ground planes based on copper and nickel perform similarly in the 40 MHz ~ 20 GHz band. The reflection response is similar enough for both ground planes that the lines are a good match to the network analyzer. The transmission response of the copper ground plane is better than the nickel ground plane above 3 GHz. There is lower loss in the nickel ground plane.

2.4   Nickel and Copper Inserts

Fig. 2.14 shows inserts that will be used to assess the performance of the microstrip line when magnetic materials are introduced to the system. The inserts fit between the FR4 dielectric layer and a Melinex dielectric layer. The inserts are placed inside the microstrip circuit because the power imparted on the insert is the cross product of the magnetic and electric fields as shown in eqn 1 and the electric fields are strongest between the signal line and ground plane.

The width and length of these copper and nickel inserts are shown in Table 2.3. Nickel insert thickness is almost twice the copper thickness as shown in Table 2.1. The microstrip line with the insert can be assumed to be a three section transmission line modeled in Fig 2.15, the center section with the insert and its associated length and characteristic impedance and the feedline sections with their own lengths and impedances. The feedline sections will have higher characteristic impedance than the line without the plastic while the insert section will have lower characteristic impedance than the feedline sections or the microstrip without plastic inserted between the ground plane and dielectric.
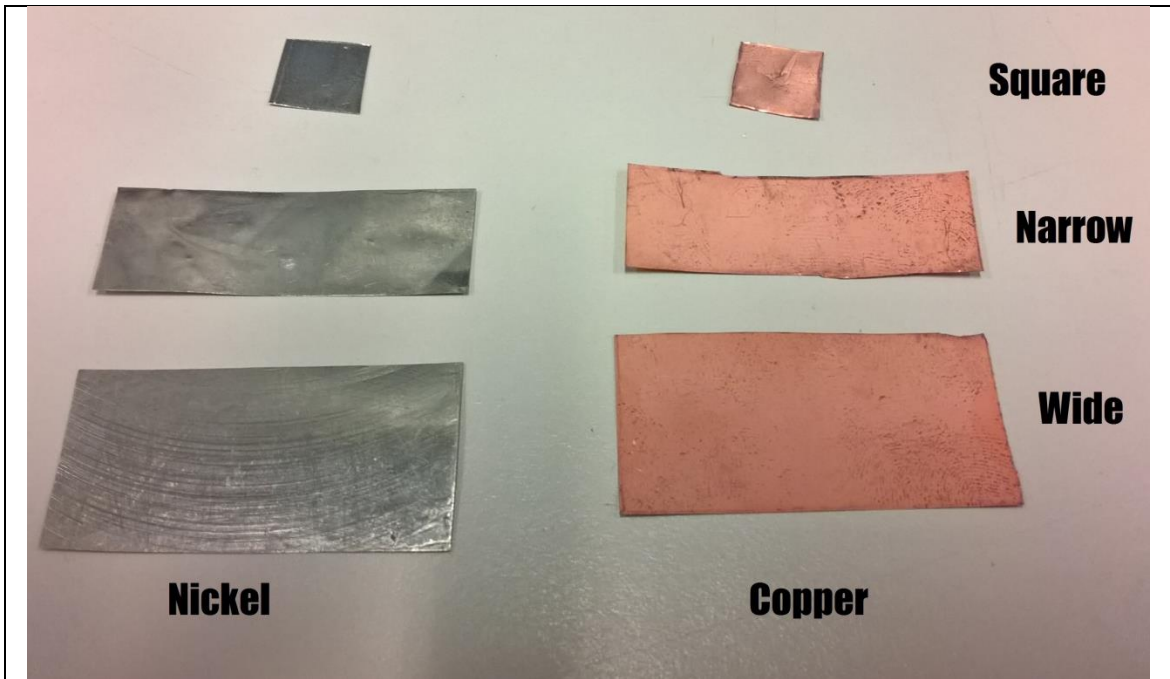
Figure 2.14 Insert materials. Clockwise from top right: Copper square, Copper narrow, Copper wide, Nickel wide, Nickel narrow, Nickel square

(a)

(b)

(c)
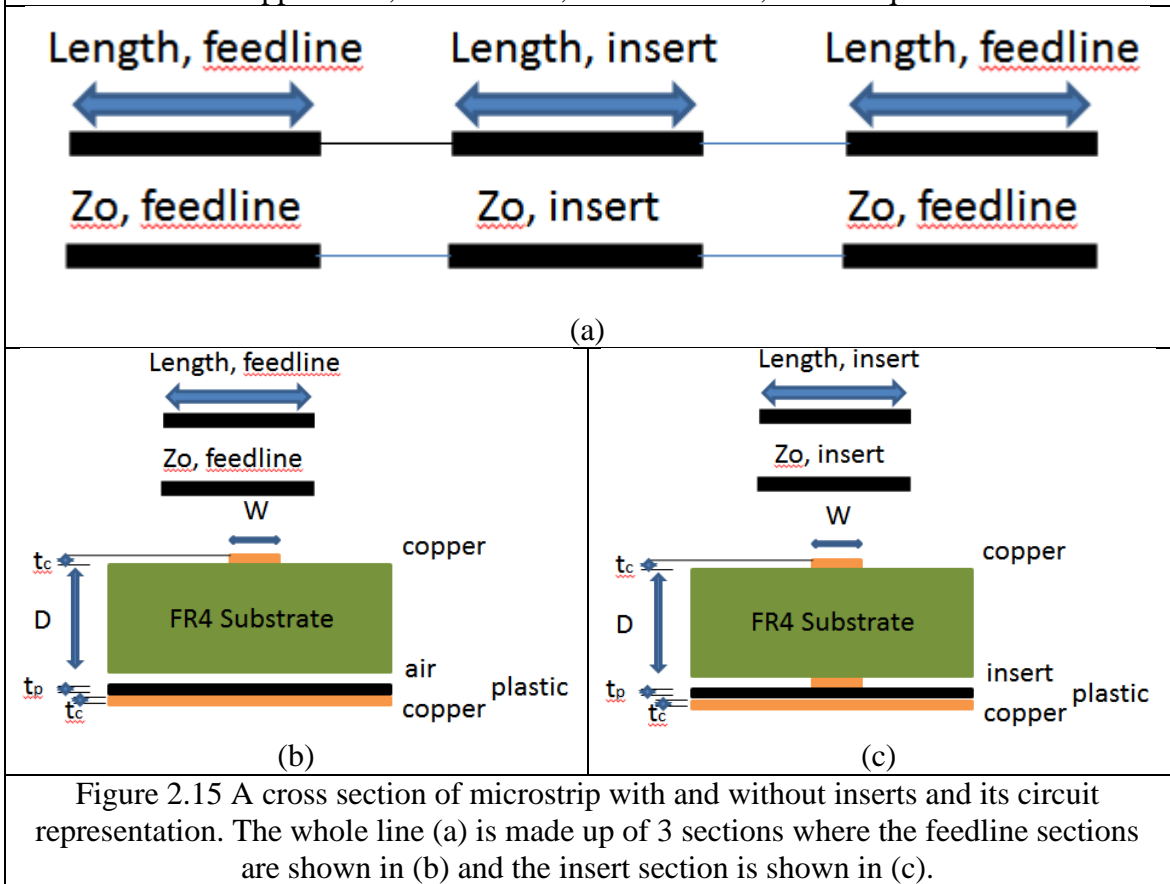
Figure 2.15 A cross section of microstrip with and without inserts and its circuit representation. The whole line (a) is made up of 3 sections where the feedline sections are shown in (b) and the insert section is shown in (c).

Table 2.3 dimensions of Nickel and Copper inserts

Insert type	Width (mils)	Length (mils)
Nickel Wide	768	1513
Nickel Narrow	525	1542
Nickel Square	417	412
Copper Wide	745	1533
Copper Narrow	538	1548
Copper Square	427	420

2.5 Nickel and Copper Insert VNA Measurements

Microstrip lines with copper or nickel inserts are discussed and compared to the conventional microstrip line design with copper or nickel ground (from Chapter 2.2). Four test circuit cases are evaluated and shown in Table 2.4. The signal line is copper in all cases. Nonmagnetic designs use Copper only; effectively magnetic designs use nickel as the insert and ground. Mixed cases use either nickel insert with copper ground (Ni insert/Cu ground) or copper insert with nickel ground (Cu insert /Ni ground). In this chapter "conventional microstrip" will be used to describe a microstrip line of either copper of nickel ground and copper signal line without an insert inside it. When the ground plane is copper the conventional microstrip has a copper ground and the same is true for nickel ground.

Table 2.4 the four cases of microstrip line and insert

Insert	Ground	
	Copper	Nickel
Copper	Non magnetic	Copper insert/Nickel ground (Cu/Ni ground)
Nickel	Nickel insert/Copper ground (Ni/Cu ground)	Effectively Magnetic

In the following chapters the wide inserts will be presented followed by the narrow inserts and then the square inserts. This is done to group similar geometries together so that the patterns that arise from the individual geometries will be apparent.

2.5.1 Wide Inserts

In Fig. 2.16a&b the nonmagnetic wide copper insert (1.89 cm wide), reflection response is relatively close to conventional microstrip up to 12 GHz. Above 12 GHz the mismatch increases, the transmission losses increase and a periodic resonance appears every 3 GHz. While the line length seems to be linked to those resonances the transmission decrease above 12 GHz corresponds to an increase in reflection response above 12 GHz, meaning less energy gets through as the mismatch increases. The 3 GHz resonances can be linked to the length of the copper insert through eqn 7. By setting the wavelength (λ) equal to the length of the insert (3.84 cm) it can be shown that the 3 GHz resonances are multiples of 1.5 wavelengths.

$$\frac{n*\lambda}{2} = \frac{c}{f*\sqrt{\mu R*\mathcal{E}eff}} \tag{7}$$

For the effectively magnetic case, shown in Fig. 2.16c&d, there are transmission nulls at 3, 6, 10, 12, and 14, 16.5 and 19 GHz. The transmission begins to drop at around 14 GHz, but it begins looking like the conventional microstrip with nickel ground. The resonances at 3, 6, 10, 14, and 19 suggest a periodic resonance at frequencies similar to the nonmagnetic case but it is not as strong.

The wide Ni insert/Cu ground case, shown in Fig. 2.16e&f, maintains the -2 dB insertion loss drop above 12 GHz that both previous wide inserts have in addition to having resonances at the same frequencies as the non-magnetic case, every 3 GHz. This measurement looks similar to the nonmagnetic transmission shown in Fig 2.16b. The reflection response shows far higher mismatch than the conventional microstrip with copper ground. The transmission nulls at 6, 9, and 12 GHz are the largest deviation from the conventional microstrip case (with the 12 GHz null being the strongest null) while the response above 15 GHz is more subdued.

The wide Cu insert/Ni ground case, shown in Fig. 2.16g&h, has transmission nulls at 2, 3, 5, 10, 12, 13, 14, and 15 GHz and looks like the conventional microstrip with nickel ground between 6 and 9 GHz and above 16 GHz. This measurement looks most like the effectively magnetic measurement shown in Fig 2.16d. The reflection response is also similar to Fig 2.16c. It can be shown that the nickel ground decreases the strengths of the resonances compared to the copper ground cases.

(a)   (b)
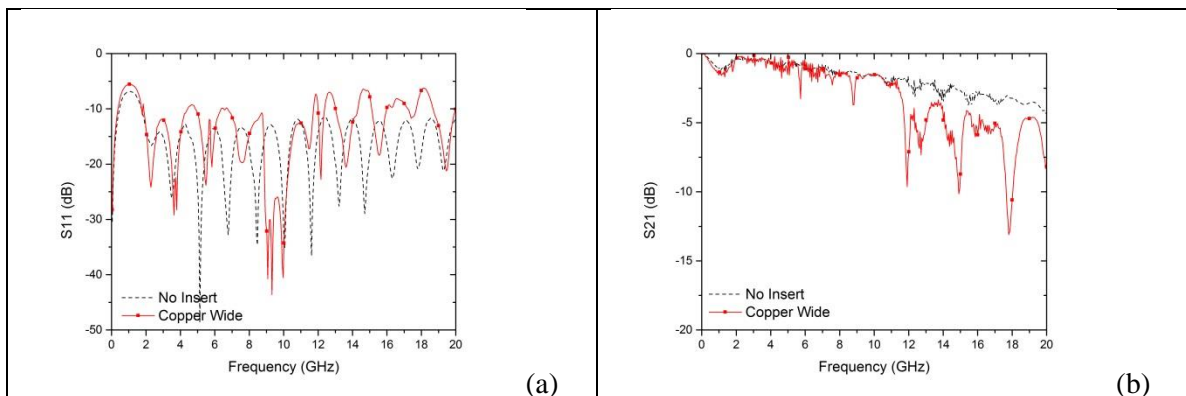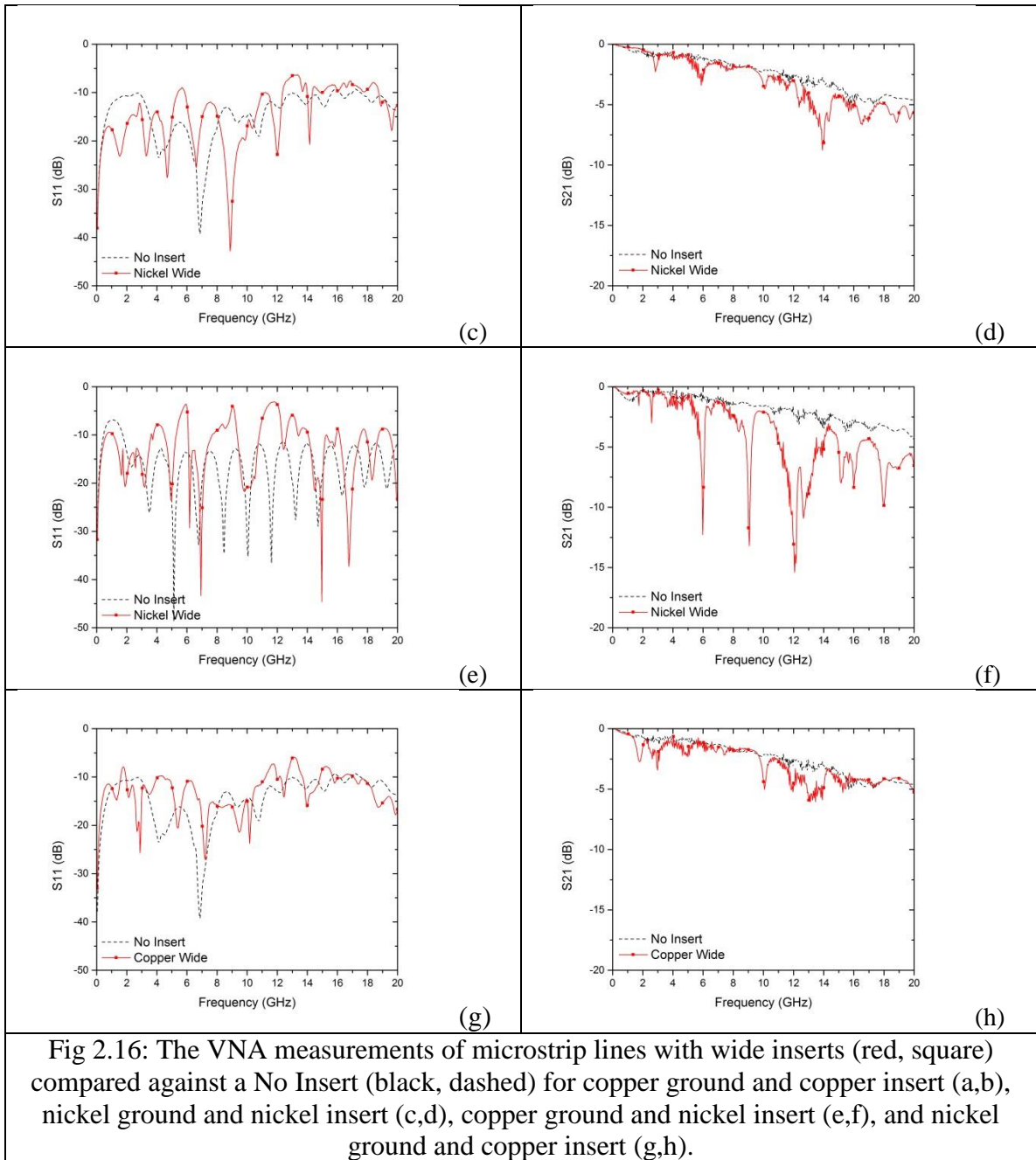
Fig 2.16: The VNA measurements of microstrip lines with wide inserts (red, square) compared against a No Insert (black, dashed) for copper ground and copper insert (a,b), nickel ground and nickel insert (c,d), copper ground and nickel insert (e,f), and nickel ground and copper insert (g,h).

Overall there is a contribution from the ground plane and the insert that can be separated and are seen across multiple measurements. The 3 GHz resonances are seen strongly in the circuits with a copper ground plane while the nickel ground plane circuits

25

have a more subdued response at shifted frequencies. The Ni insert/ Cu ground case had the largest difference from the conventional microstrip at 12 GHz.

2.5.2 Narrow Inserts

In Fig. 2.17a&b the narrow copper insert (1.37 cm wide) transmission response shows reduced periodic resonances and highest loss above 16 GHz. The transmission response has resonances at 2, 2.8, 5, 5.8, 7, 8.4 and 10.7 GHz before it begins fluctuating 2 dB up and down. Since the narrow insert is the same length as the wide insert there should be 3 GHz resonances in this structure and aside from the lack of a resonance at 9 GHz, this circuit also maintains the resonances linked to its length. Above 16 GHz the transmission response drops 2 GHz below the conventional microstrip with copper ground, but it still has resonances at 17 and 19 GHz. When compared to the copper wide measurement the strongly periodic nature of the resonances do not persist (suggesting that the periodicity is related to insert width), but the decrease in transmission above 16 GHz in both cases suggests that the transmission decrease may be due to length.

The effectively magnetic narrow insert, shown in Fig. 2.17c&d, is similar to the conventional microstrip with nickel ground, showing nulls at 2.5, 12.5, and 17 GHz and small deviations from transmission beside that. When compared against the nonmagnetic case (Fig 2.17a&b) it has neither the 2, 5, 5.8, or 7 GHz resonances nor the strong deviation from conventional microstrip above 12 GHz, but the 3 GHz effectively magnetic resonance and the 2.5 GHz nonmagnetic resonance seem to be in about the same place.

26

The narrow Ni insert/Cu ground case, shown in Fig. 2.17e&f, the narrow mixed metal case more closely matches the effectively magnetic case with resonances at 2.74, 8.92, 11.1, 12, 14.1, 16.9, and 19.6 GHz. The narrow Ni/Cu ground case is similar to the effectively magnetic transmission shown in Fig. 2.17d with a null at 3 GHz with resonances above 9 GHz that are larger in the Ni/Cu ground transmission.

The narrow Cu insert/Ni ground case, shown in Fig. 2.17g&h, looks like the nonmagnetic measurement shown in Fig 3.10b. There are resonances at 2, 2.7, 5, 5.8, 7, 9, 11, 14, and 16 GHz before the transmission response drops 2 dB before resonances at 18, 18.7, and 19.5 GHz. The 2, 2.7, 5, 5.8, 7, and 11 GHz resonances are similar between the nonmagnetic and Cu/Ni ground and only a resonance at 9 GHz in the Cu/Ni ground and 8.2 GHz in the nonmagnetic case are at different frequencies.

(a)   (b)

Fig 2.17 The VNA measurements of microstrip lines with narrow inserts (red, square) compared against a No Insert (black, dashed) for copper ground and copper insert (a,b), nickel ground and nickel insert (c,d), copper ground and nickel insert (e,f), and nickel ground and copper insert (g,h).
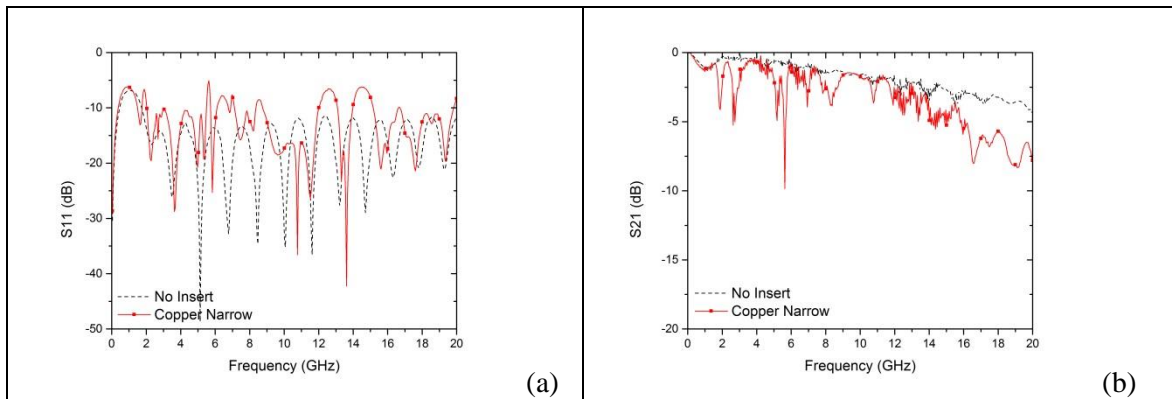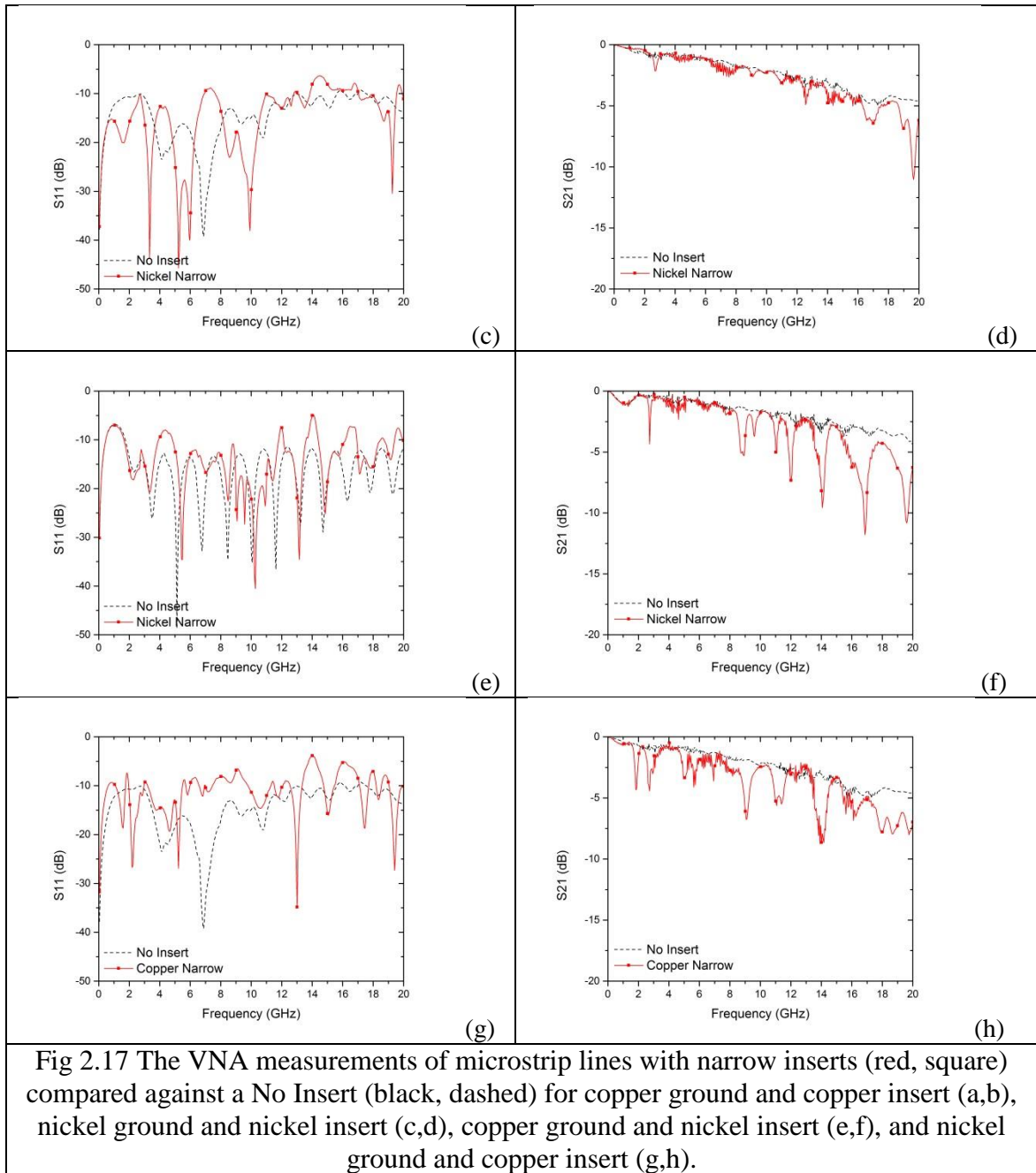
Overall the narrow insert behaves similarly to the wide insert, but there are more resonances in the low frequencies, likely due to the narrower width. The nickel ground

still subdues the transmission response. The effectively magnetic case (2.17c&d) shows the least change with the insert's inclusion.

2.5.3 Square Inserts

In Fig. 2.18(a&b) the square copper insert (1.08 cm wide) transmission response matches the microstrip most consistently across the band above 3 GHz. The resonances below 7 GHz are similar to resonances in the narrow insert measurement below 7 GHz which suggest the line width may be responsible for the low band resonances. When the length of the square insert (1.05 cm) is substituted in for the wavelength of (2) the resonances correspond to 8 times the wavelength, far too large to not see something at lower frequencies. Above 7 GHz the square insert measurement behaves like the conventional microstrip with copper ground, suggesting that length determined the drop in transmission above 7 GHz.

The square insert, shown in Fig. 2.18(c&d), has two wide transmission nulls at 4 and 13 GHz where both are significantly wider than the nulls that have come before them. When compared against Fig. 2.18b they are extremely dissimilar and do not match to each other, the two nulls in the effectively nickel measurement do not match to any null in the nonmagnetic measurement and vice-versa.

The square Ni insert/Cu ground case, shown in Fig. 2.18(e&f), more closely matches the effectively magnetic case in Fig 2.18d with a deep resonance near 11 GHz (13 GHz for effectively magnetic) and a strong similarity to the conventional microstrip

case. The resonance at 13 GHz dropped 2 GHz and the 4 GHz resonance dropped to 3 GHz and is much lower in magnitude.

The square Cu insert/Ni ground case, shown in Fig 2.18(g&h), looks like the Ni/Cu ground measurement shown in Fig 2.18f and the effectively magnetic case in Fig 2.18d. The resonance at 11 GHz is at the same frequency as the Ni/Cu ground while being ~2 GHz lower than the effectively magnetic case. The increase in transmission above the conventional microstrip with nickel ground between 2 and 10 GHz and above 12 GHz is unusual when the reflection response is about the same between the conventional microstrip with nickel ground and this Cu/Ni ground square insert case. The nulls in transmission below 8 GHz look like the nonmagnetic case (Fig. 2.18a&b) and that is linked to the insert being nonmagnetic.

(a)   (b)
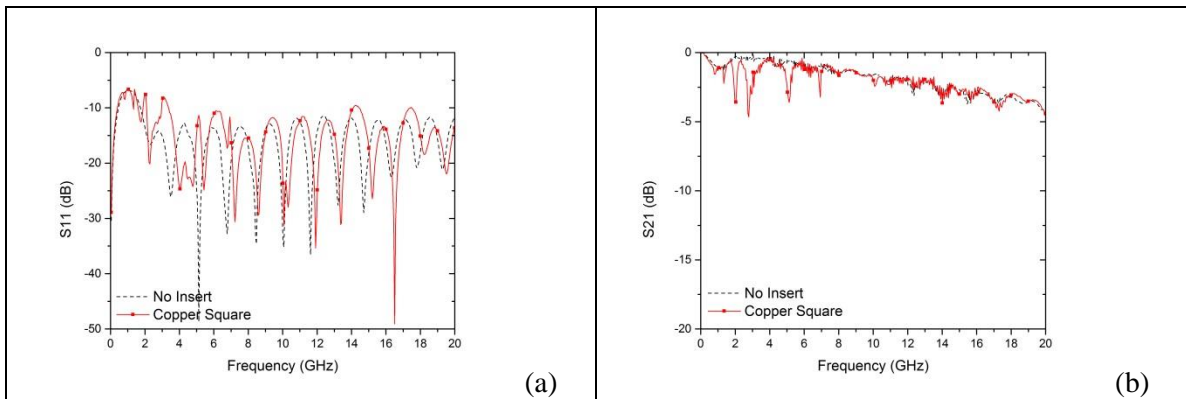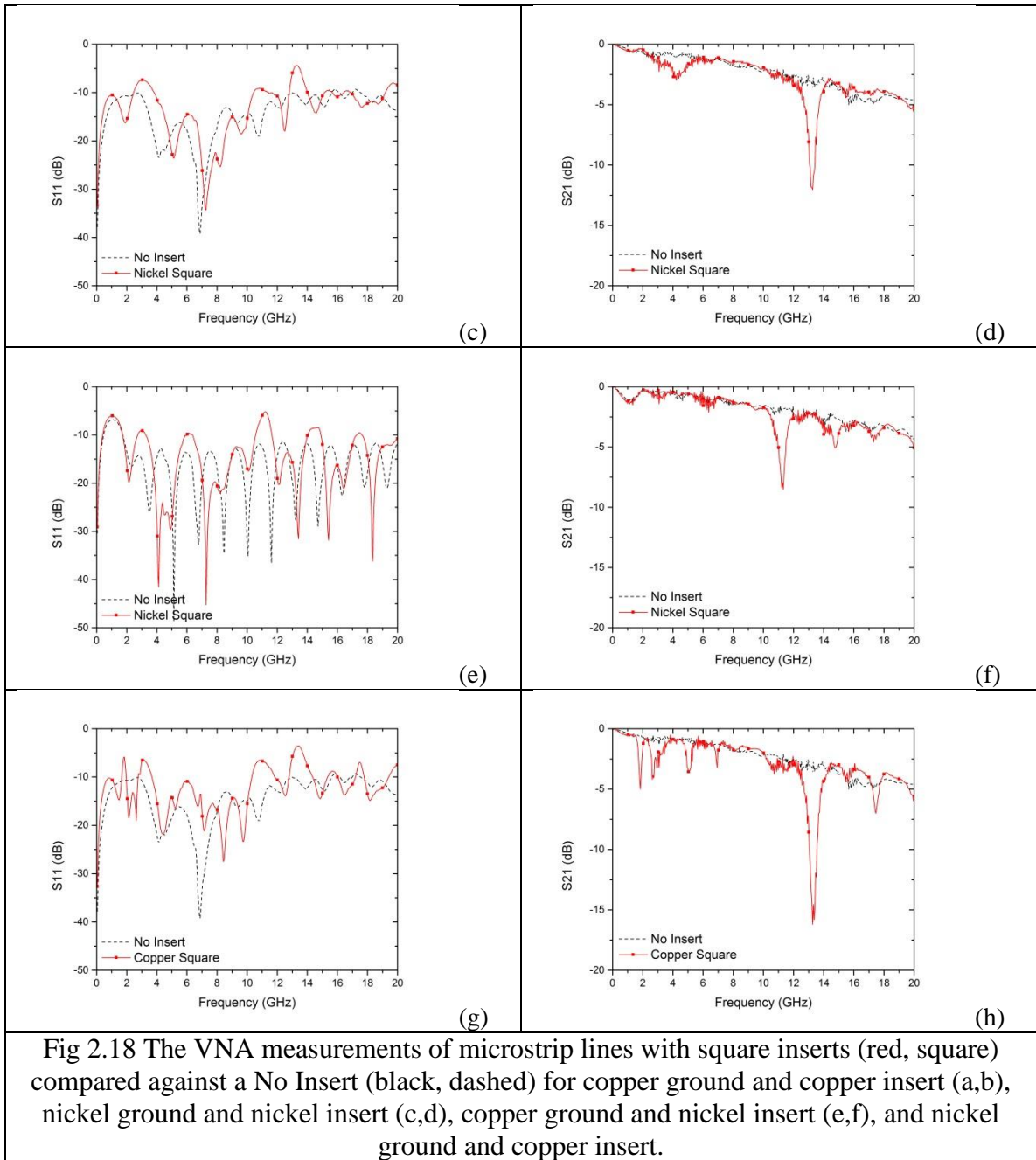
Fig 2.18 The VNA measurements of microstrip lines with square inserts (red, square) compared against a No Insert (black, dashed) for copper ground and copper insert (a,b), nickel ground and nickel insert (c,d), copper ground and nickel insert (e,f), and nickel ground and copper insert.

Overall the square insert shows fewer resonances than either the wide or narrow inserts. The transmission nulls in the low frequency are linked to the copper insert and the nulls in the higher frequency are linked to the presence of any magnetic material.

31

2.5.4 Insert Comparison Conclusion

When an insert is added to a conventional microstrip, the length and width impact transmission and reflection response by changing the impedance of the line and by changing the transmission mode. The measurements performed in this chapter proved that there are 2 sorts of resonances: those defined by the length of the insert and those defined by the width of the microstrip.

The width of the insert defines the transmission of the microstrip line by adding specific resonances to it. The width of the insert defines the 3 GHz resonances in 2.5.1's Fig 2.16b and Fig 2.17f as roughly every 3 GHz, but this only occurs with a copper ground plane. For the narrow case there are many resonances that can be linked to specific designs, such as the 2~7 GHz range between 2.5.2's Fig 2.17b and Fig 2.17h linked to the copper insert or the 9~20 GHz range between 2.5.2's Fig 2.17f and Fig 2.17h that do not share a ground plane or insert metal. When the width is reduced to the square insert's ~420 mils those resonances disappear.

The length of the inserts also determines how the circuits look, especially when one compares the wide and narrow insert measurements (which have roughly the same length) to the square insert. The square insert measurements will have one or two large transmission resonances while wide or narrow insert measurements have many narrow resonances.

2.6   Nickel and Copper insert models

Chapter 2.5 characterized how microstrip lines perform with inserts within them, and this chapter aims to replicate those measurements with the simulation tools from chapter 2.3. A full discussion is in Appendix B, but the results will be briefly covered here. Fig 2.19 shows the Copper ground microstrip with a wide copper insert when it's measured on the VNA (black, dashed), when it's simulated in HFSS (red, square) and when it's simulated in ADS (blue, x). Neither HFSS nor ADS accurately model either the recurring 3 GHz transmission nulls or the reflection response, but both are an adequate predictor of the of the transmission response before the nulls are applied. Overall the models are not capable of capturing the transmission nulls from the VNA measurements and cannot be used to predict the response of the microstrip lines.

(a)	(b)

Figure 2.19 Reflection and transmission response of the copper wide insert on copper ground microstrip for VNA Measurement (black, dashed) vs HFSS model (red, square) and ADS model (blue, x)
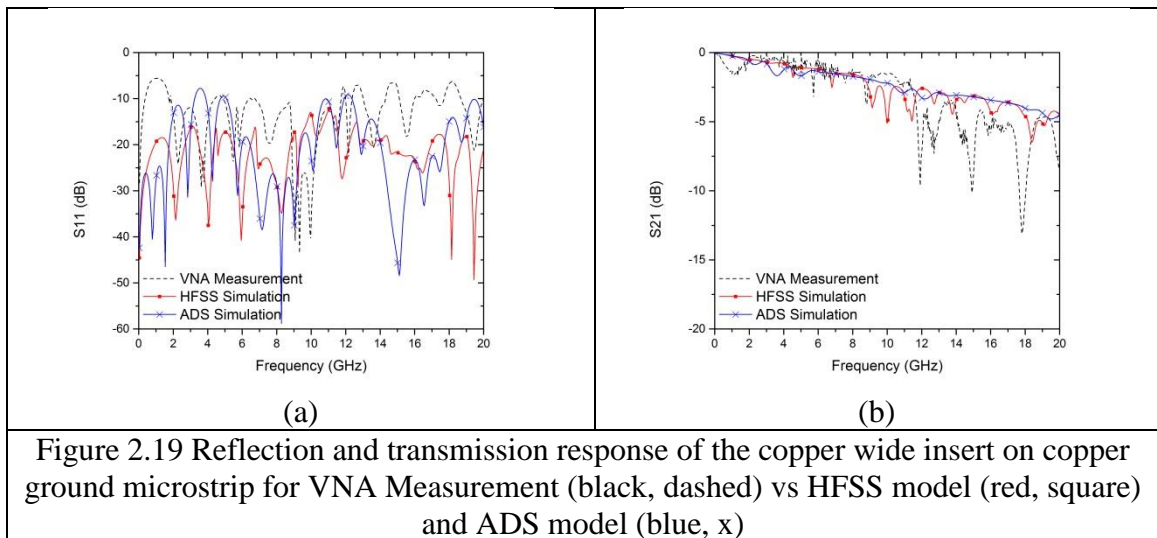
2.7   Conclusion

Adding inserts to the transmission lines radically changes how they operate by changing how signals propagate through circuits. The inserts are placed between the

dielectric substrate and the ground plane in order to ensure that the insert is exposed to both electric and magnetic fields and can thus absorb power. Magnetic and Nonmagnetic materials are used for the insert to determine the influence of magnetic materials (copper and nickel), and the resulting measurements are different from each other. VNA Measurements show a dependence of the reflection and transmission response on the length and width of the insert along with the insert's material composition. Various simulation tools were applied to replicate the performance of the microstrip lines with inserts, but they could not replicate the measurements. This chapter characterized microstrip lines with inserts, and next chapter will apply magnetic fields.

Chapter 3: DC Magnetic Field Effects on Microstrip Lines

3.1 Introduction

This chapter characterizes the circuits from chapter 3 with both AC and DC magnetic field biases. Previous work has measured FMR with SQUID ([20]), Vibrating Sample Measurement (VSM) ([6], [21], [24]), and VNA-FMR ([2], [7], [10], [12], [15], [16], [17], [19], [25]). VNA-FMR was used in this work because it used the same VNA as chapter 2. The DC magnetic field will be applied by an external magnetic field while the AC magnetic field will come from the VNA used in Chapter 2. By exposing the metallic inserts to a DC magnetic field a phenomenon called ferromagnetic resonance (FMR) is expected to occur that will absorb power from the AC magnetic field and disturb the transmission of the microstrip circuit [2].

3.2 SMA connectors and microstrip test circuits

The circuits shown in Fig. 3.1 have SMA connectors [40] soldered onto them. These circuits have the same dimensions as those in chapter 2's Table 2.1 and Table 2.2, but with the SMA connector soldered to the signal line and ground plane. The metal inserts slide between the plastic and FR4 dielectric layers and are visible through the dielectric substrate so they can be properly aligned by sight. The square inserts are small enough that they need to be taped to a sheet of Melinex plastic for accurate alignment, so there is another layer of Melinex in the square insert measurements.

Figure 3.1 (a) microstrip lines with SMA connectors (b) metal inserts from chapter 3, with their dimensions defined in Table 2.3 and the nickel square taped to a sheet of Melinex
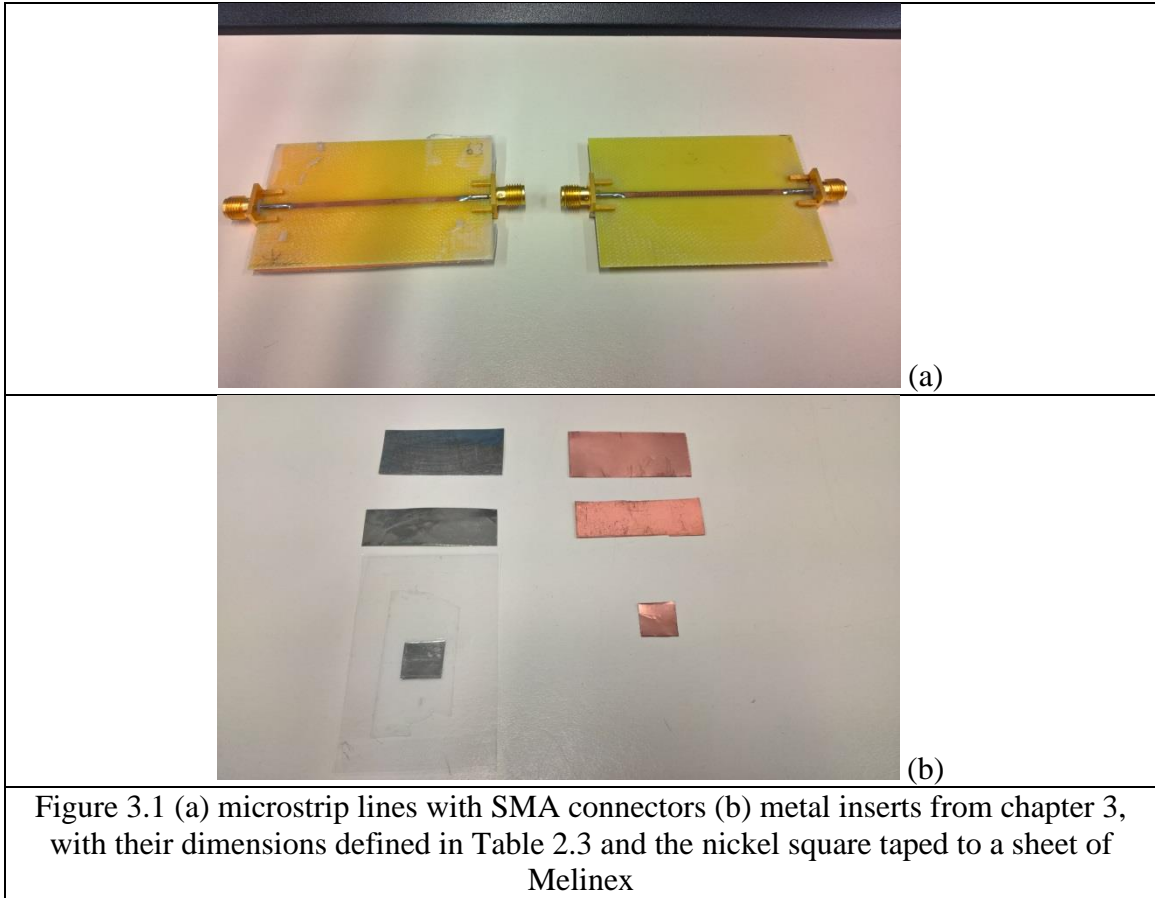
These microstrip circuits will be used with the VNA, but these new lines with their SMA connectors need to be characterized. The Anritsu VNA from Chapter 2 is used to characterize the microstrip circuits with SMA connectors by evaluating the S-parameters using SOLT calibration. As in chapter 2, reflection and transmission responses are displayed in Fig 3.3 and the impedance is calculated from those measurements and shown in Fig 3.2. Despite the incremental impedance mismatch; both measurements are generally below -10 dB for return loss. The transmission response slightly decreases when compared to similar data from the UTF measurements from Chapter 2. The transmission response in Fig. 3.3b, at 20 GHz, is 1 dB lower than the

equivalent UTF measurements. The transmission resonance at 8.873 GHz and 7.774 GHz in the transmission response is due to the SMA connector.
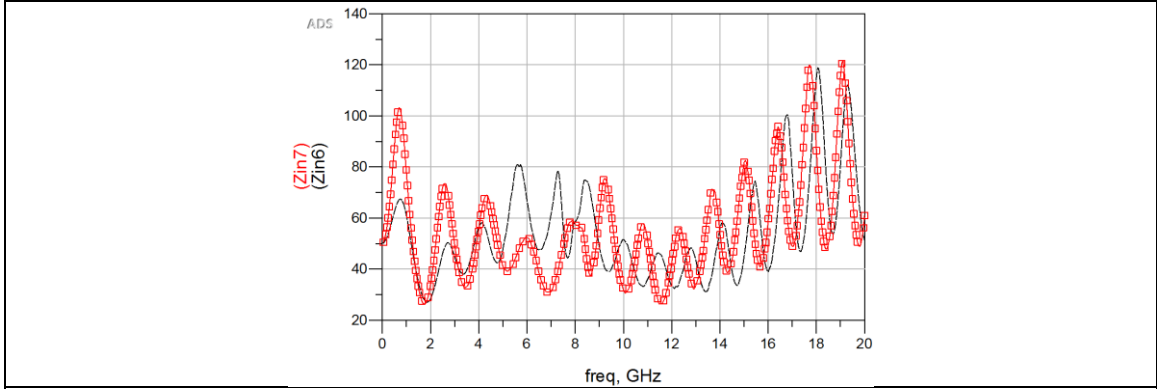
Figure 3.2 Measured with SMA connectors for copper (red) and nickel (black, dashed) ground impedances

(a)   (b)
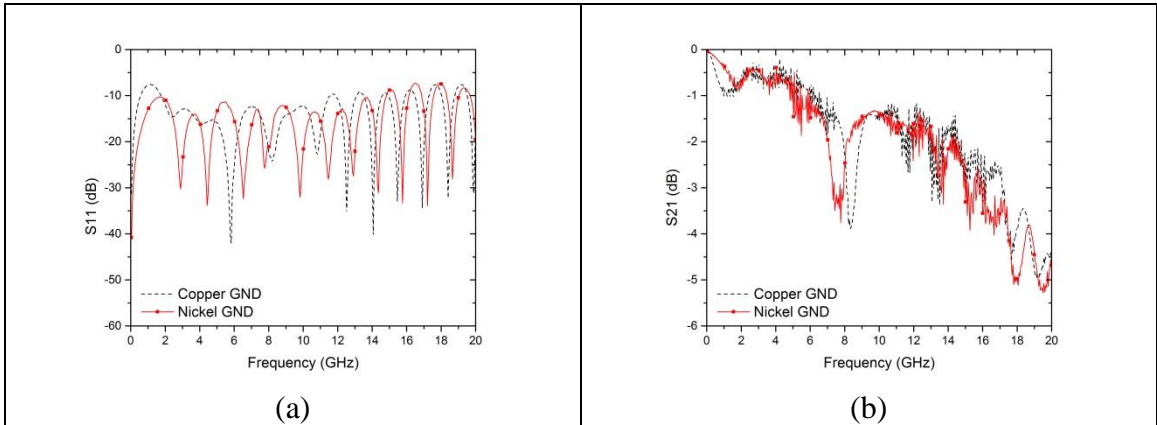
Figure 3.3 The reflection (a) and transmission (b) response of microstrip with copper GND (black, dashed) and nickel GND (red, square) for the circuits in Fig. 3.1.

The SMA is rated to 18 GHz and the transmission responses above that reduce by 1.5 dB as seen in Fig. 3.3. All DC plus AC data will be measured up to 18 GHz. The transmission nulls at 7.7 and 8.8 GHz are not reflected in the impedance plot.

3.3   Measurement Setup with VNA and DC Magnetic Field

In this chapter, the microstrip lines are evaluated with AC and DC magnetic fields. The AC fields are provided by the VNA and DC fields provided by a Vibrating Sample Measurement (VSM) repurposed to serve as an external electromagnet. Fig 3.4a shows the measurement setup with the electromagnet, VNA, and laptop that controls the VNA. The VNA provides the AC signal and is swept from 4 GHz to 18 GHz. No calibration is used with the VNA in this configuration. An in-house MATLAB script [41], [42] is used to control the electromagnet and VNA sweep and will capture measurement data. The VSM cores are shown in Fig 3.4b. They provide the magnetic flux between the two plates as shown in Fig 3.4c. The magnetic field is strongest in the center of the plates. The plate used in these test are 2 inches in diameter at their narrowest. The test circuits to be measured are 2372 mils (60.23 mm) by 1502 mils (38.16 mm). The metal inserts considered have the following widths: 768 and 745 (wide), 525 and 538 (narrow), or 417 and 420 (square).

Figure 3.4a Electromagnet, VNA, and Laptop
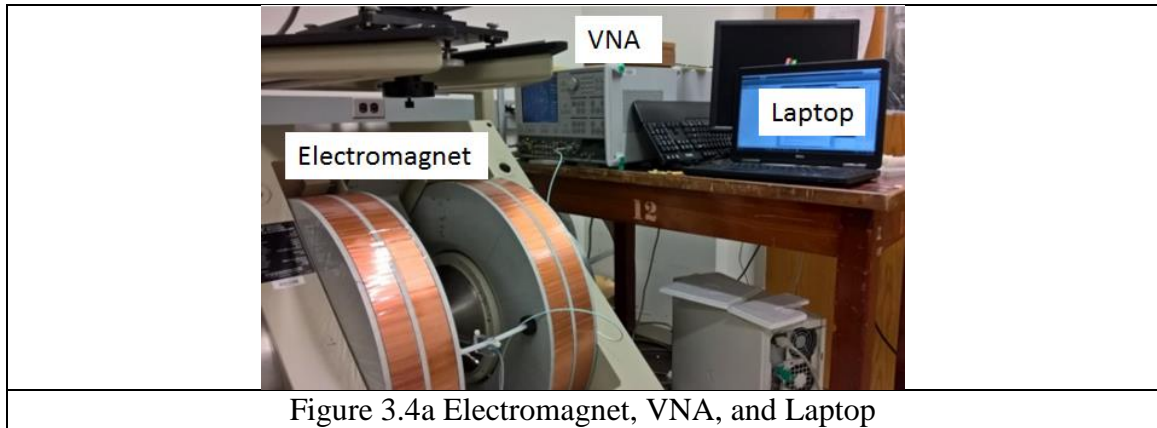
Figure 3.4b the Electromagnet core with VNA cable
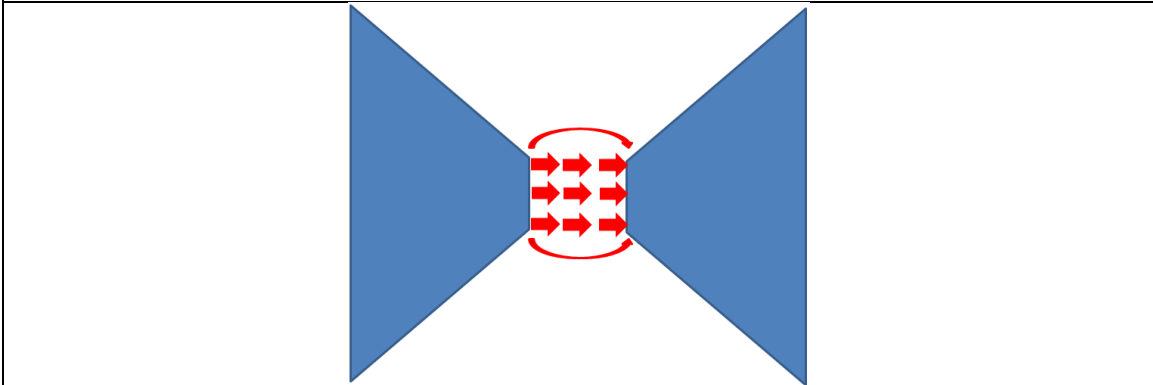
Figure 3.4c magnetic field direction inside Electromagnet's cores

The electromagnet's DC magnetic field is swept from +15 kOe to -15 kOe and back. Fig 3.5a shows the microstrip DUT inserted into the electromagnet on a polystyrene holder. Fig. 3.5b shows the foam spacer that is added to hold the circuit in the same position when the magnetic field is on. The polystyrene foam does not interfere with the magnetic fields. The DC magnetic field excitation can be applied either perpendicular or parallel to the signal line based on the microstrip's orientation. In this work, perpendicular DC fields are used. The DUT is placed parallel to the electromagnetic plates and in the center of the two plates in order to provide a uniform DC magnetic field perpendicular to signal line and ground plane.

Figure 3.5a a microstrip test circuit inside the Electromagnet

Figure 3.5b the microstrip test circuit inside the Electromagnet with spacers to hold it in place.

Chapter 2 measurements were swept frequency from 40 MHz to 20 GHz. In this chapter measurements are up to 18 GHz and uncalibrated. The calibration from Chapter 2 cannot be applied to the circuits in this chapter because the single frequency operating mode of the VNA to take these measurements only functions while uncalibrated. Additionally, all RF frequency data is measured by an in house program. Fig. 3.6 is a plot of calibrated (SOLT with SMA) and uncalibrated (SMA) microstrip data for reflection and transmission response. The reflection responses resemble each other, but the uncalibrated measurement contains more noise. Below 8 GHz the uncalibrated transmission response is above zero (>1) due to the uncalibrated nature of the VNA

system. Most data in this chapter will be presented as linear values instead of dB as in chapter 3.

(a)   (b)

Figure 3.6 calibrated (black, dashed) vs uncalibrated (red, squares) microstrip with copper GND and SMA connectors
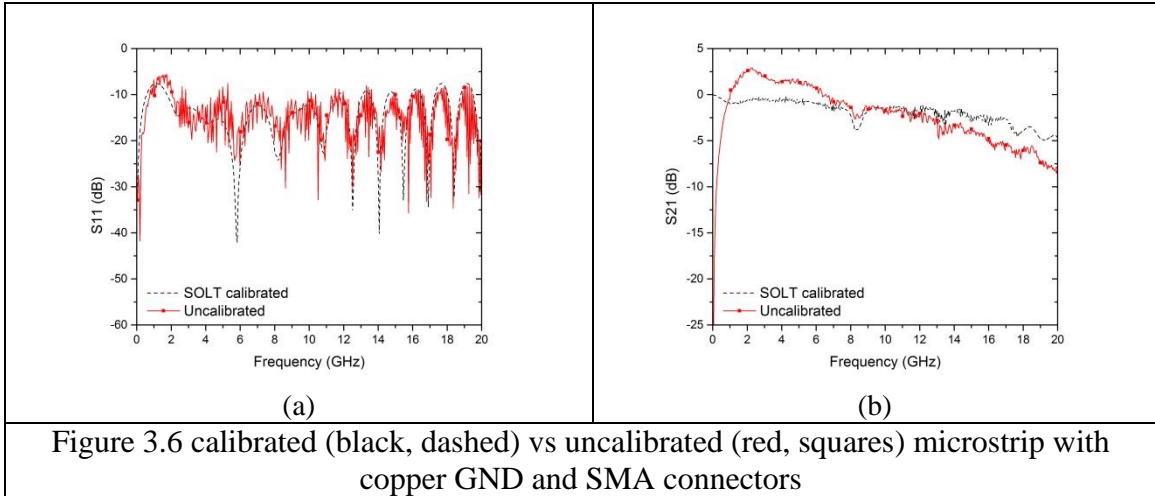
DC magnetic field measurements are taken for a given RF frequency from 2~18 GHz in 2 GHz increments. Table 3.1 shows the transmission response at those frequency points based on the linear data in Fig. 3.7.

Figure 3.7 The transmission coefficient of uncalibrated (red) and calibrated (blue) VNA measurements of the copper ground microstrip transmission line.
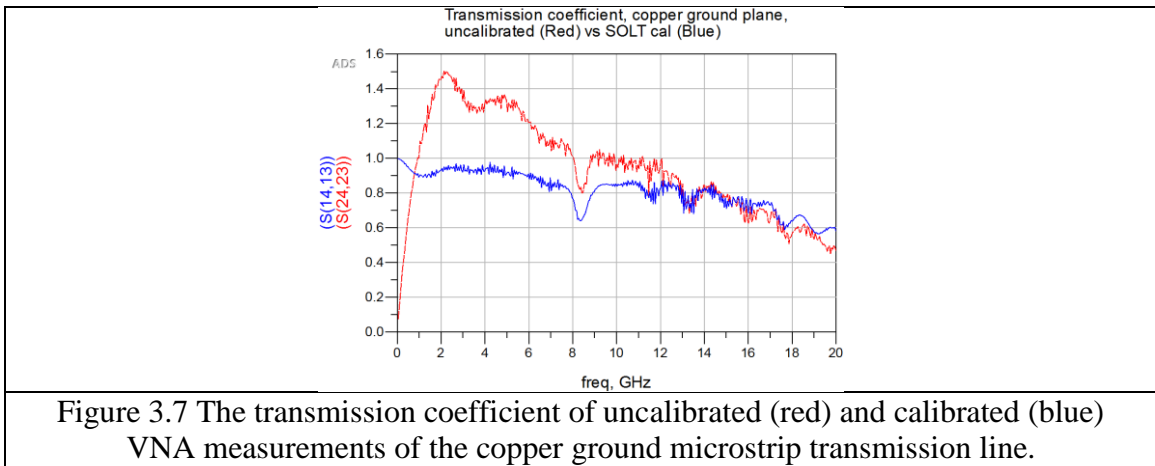
Table 3.1 Linear values of the Transmission Coefficient of the Copper Ground for calibrated and uncalibrated data

Freq	2 GHz	4 GHz	6 GHz	8 GHz	10 GHz	12 GHz	14 GHz	16 GHz	18 GHz
S21 (cal)	0.929	0.925	.910	0.763	0.838	0.829	0.83	0.682	0.637
S21 (no cal)	1.45	1.31	1.20	1.00	0.96	0.98	0.84	0.62	0.56

3.4   Measurement Methodology

The microstrip lines with SMA connectors will be placed in the electromagnet to apply a DC B-field and the VNA will be used to measure the circuit while the DC B-field is swept [15], [25]. The DC B-field is applied perpendicularly to the metal insert and ground plane of the microstrip line, as shown in Fig. 3.8. Since the DC B-field is perpendicular to the face of the electromagnet the ground plane and insert are parallel to the face of the electromagnet. The magnetization axis of the metal insert is in the plane of the insert, so the DC B-field is accessing the hard-axis of the metallic insert. Only the copper ground plane microstrip line will be measured with the strong magnetic fields to avoid damaging the nickel ground plane with the strong magnetic field bending or removing the ground plane from the circuit.

Figure 3.8 The configuration of the AC and DC B (H) fields on the microstrip circuit

42
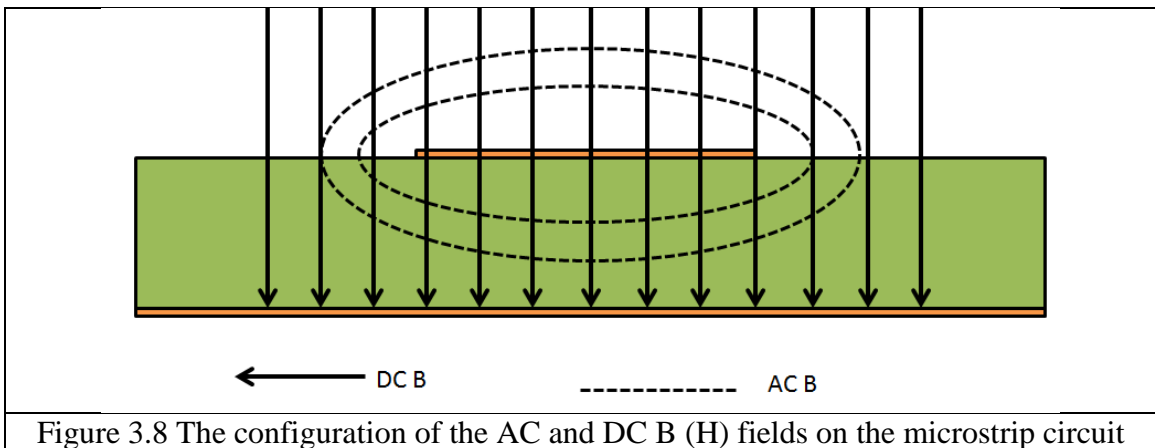
The electromagnet is programmed to sweep the DC B-field from +15 kOe down to -15 kOe in 3 minutes while the VNA is measuring the circuit at a constant frequency before rising from -15 kOe to +15 kOe in 20 seconds while the VNA switches frequency. The VNA starts at 18 GHz then shifts down by 2 GHz, and then repeats the measurement until it reaches 4 GHz. During this time the VNA and electromagnet desynchronize and over time the 0 kOe point moves as the frequencies shift. This shift is given in Table 3.2 as the electromagnet slows down when compared to the VNA. The X's in Table 3.2 are where there is little variation with magnetic field and the 0 kOe point is indeterminable.

Table 3.2: DC B-field 0 kOe shift at each frequency for nickel inserts

F (GHz)	4 GHz	6 GHz	8 GHz	10 GHz	12 GHz	14 GHz	16 GHz	18 GHz
Wide (kOe)	-5.01	-4.19	-3.51	-2.61	-1.77	-1.01	0	+0.45
Narrow (kOe)	-5.07	-4.2	-3.39	-2.53	-1.77	X	-0.09	+0.334
Square (kOe)	-5	-4.07	-3.37	-2.63	X	-1.03	-0.27	+0.57

A nanowire sample with a known FMR will be tested to show the drift of the VNA. The Nanowires used in this chapter are Cobalt nanowires with an expected FMR frequency of 8 GHz with 0 externally applied B-Field. The Nanowire samples are built through an AAO substrate that is 1 square centimeter in size, then cut down to match the nanowires. The AAO substrate with the nanowires built into it is attached onto the microstrip line, shown in Fig 3.9. The nanowire sample was so fragile that it couldn't be inserted between the ground plane and the dielectric without it breaking, so the nanowire sample was affixed with vacuum grease on top of the circuit as seen in Fig. 3.11. The

DUT will be inserted parallel to the plates of the Electromagnet as described in chapter 3.3.

Figure 3.9 nanowire sample affixed to microstrip line
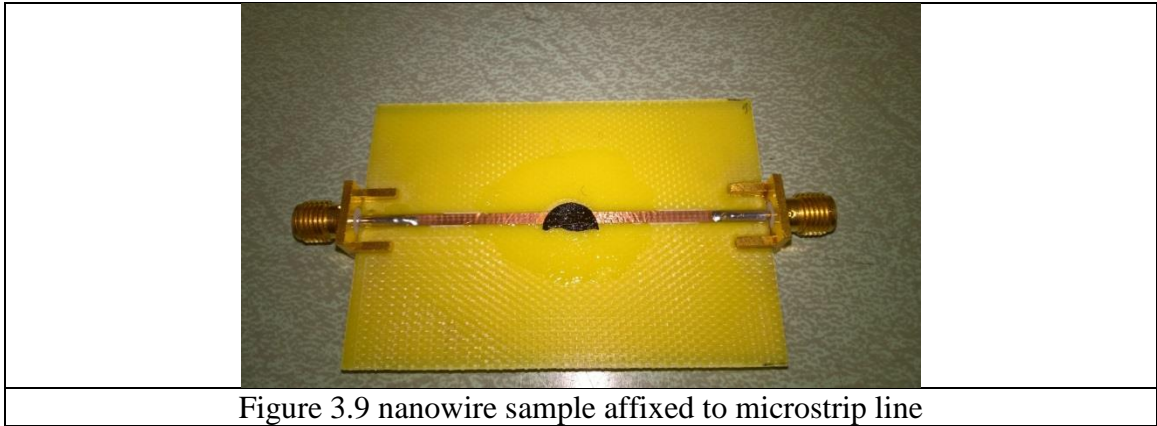
The results of the magnetic field sweep are plotted as a family of curves and shown in Figs. 3.10 and 3.11. Fig 3.10 shows the measured data with no averaging while the data from Fig. 3.11 has been averaged and then arranged by frequency. There is little change in transmission with magnetic field strength. At zero kOe the attenuation decreases for the corresponding RF frequencies in order of 4, 6, 8, 10, 12, 14, 16 and 18 GHz. The nanowires could not display the FMR expected of them, but the transmission decreases when no magnetic field is applied. That decrease in transmission shows the shift in the zero point over time, where the shift in the 0 point can be seen with the first measurement at 18 GHz at 0.45 kOe that then shifts down to -5 kOe at 4 GHz. Also starting at 10 GHz the rising cycle of the magnetic field passing through 0 kOe is captured at 15 kOe on the plot and it decreases in frequency with the falling cycle of the sweep passes through 0 kOe. The nanowire measurements have shown that the 0 point of the sweep moves over time and have characterized how the 0 point moves.
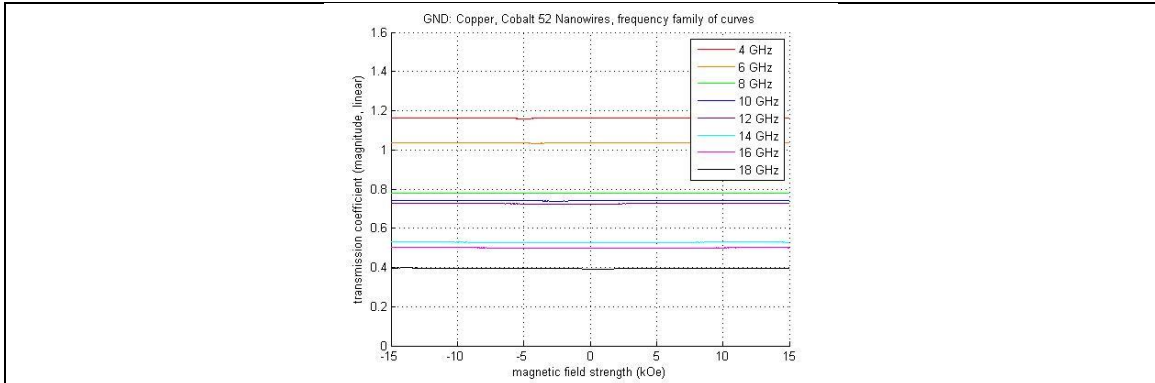
Figure 3.10 copper ground, cobalt 52 nanowires, family of curves
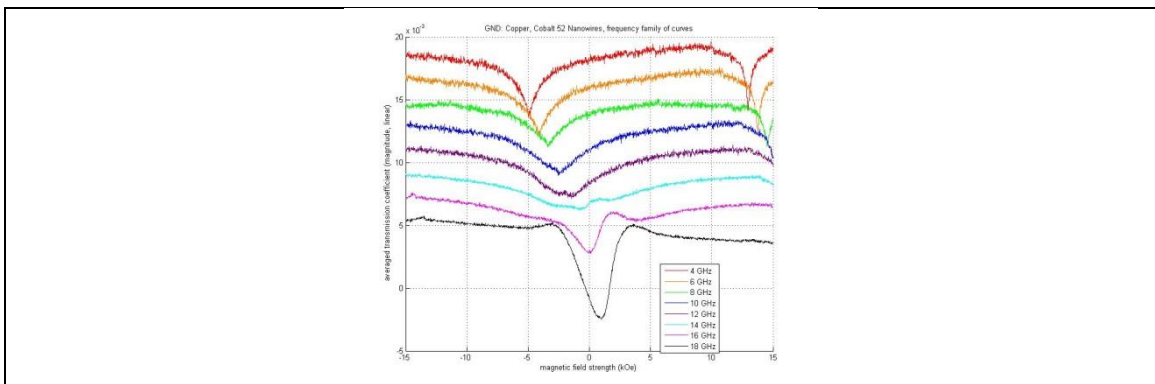
Figure 3.11 copper ground, cobalt 52 nanowires, family of curves, averaged

3.5   DC B-Field Measurements

DC magnetic fields will be applied to microstrip lines with and without inserts in this chapter. The objective is to characterize the response of the inserts when DC and AC magnetic fields are applied simultaneously. Before any DC B-field is applied the uncalibrated circuits were measured. Figs. 3.12 and 3.13 shows the AC only transmission response of the SMA copper ground microstrip over the frequencies measured for copper and nickel inserts respectively and this data is also shown in Table 3.3. This baseline data without DC B field in Fig. 3.12 indicates that there are specific resonances in the copper

45

inserts such as 6 GHz for the copper wide 10 GHz for the copper square. The nickel data in Fig. 3.13 shows a resonance at 6 GHz for the wide and narrow inserts and the square insert stays close to the no insert case. The baseline measurements were made with the copper ground plane. With the magnetic materials it is expected that if the nulls in transmission data move to higher or lower frequencies with applied DC bias field the null may represent the ferromagnetic resonance of the material. So the copper inserts should remain constant over the B field sweep compared to the nickel inserts, which should change with magnetic field strength.

Figure 3.12 the transmission response of uncalibrated SMA copper ground plane microstrip with no insert and copper inserts at the measurement frequencies with no DC B-field

Figure 3.13 the transmission response of uncalibrated SMA copper ground plane microstrip with no insert and nickel inserts at the measurement frequencies with no DC B-field
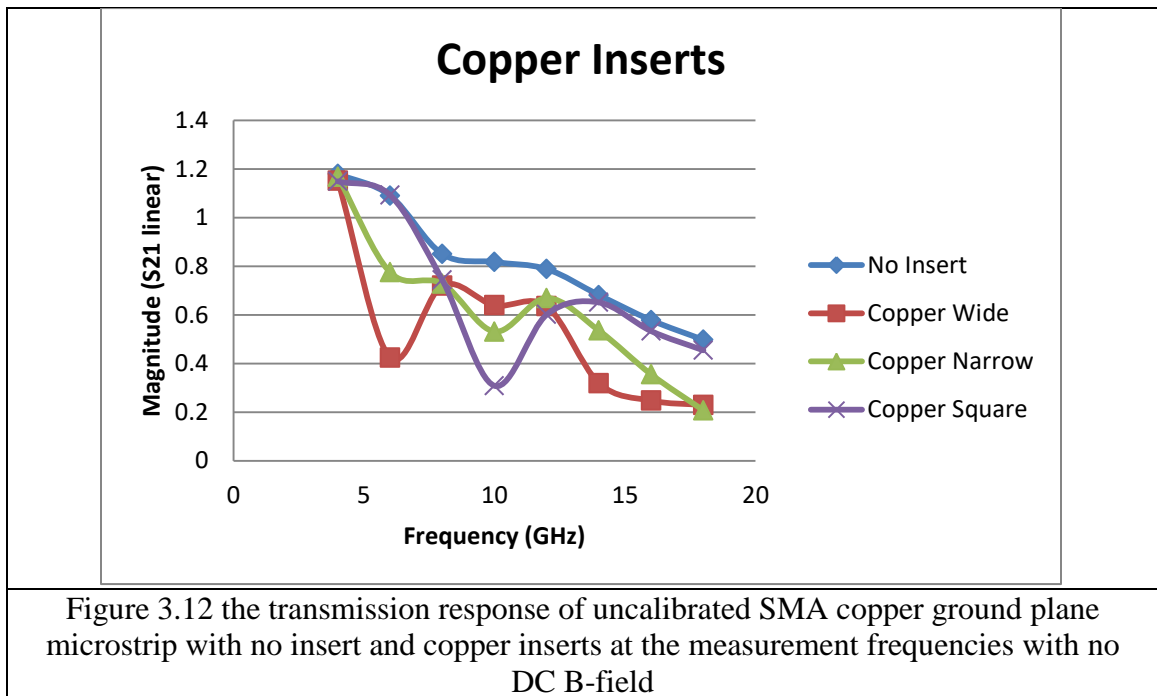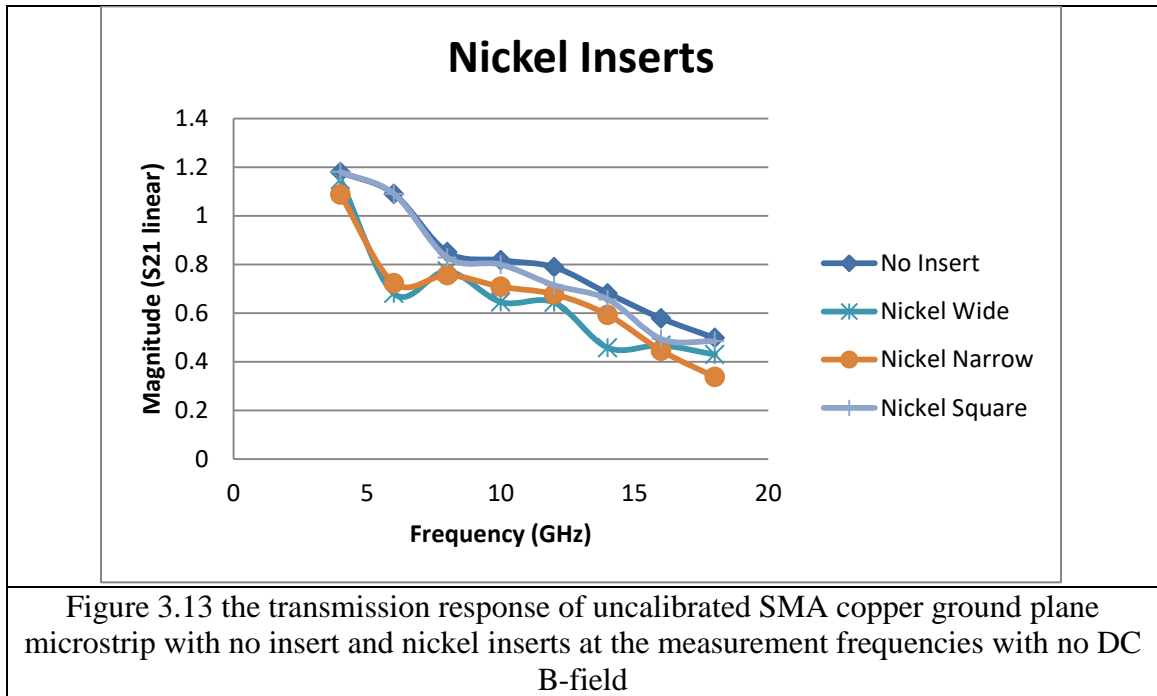
Table 3.3 Uncalibrated transmission values for varying samples at 0 kOe on a microstrip with Copper GND plane and SMA connectors.

	No Insert	Copper Wide	Copper Narrow	Copper Square	Nickel Wide	Nickel Narrow	Nickel Square
4	1.179	1.152	1.167	1.149	1.148	1.087	1.18
6	1.09	0.424	0.775	1.092	0.68	0.723	1.09
8	0.85	0.72	0.728	0.743	0.772	0.756	0.828
10	0.817	0.639	0.531	0.308	0.645	0.708	0.799
12	0.788	0.635	0.669	0.601	0.643	0.677	0.714
14	0.681	0.319	0.535	0.651	0.457	0.592	0.656
16	0.578	0.247	0.355	0.533	0.467	0.445	0.493
18	0.497	0.229	0.207	0.454	0.429	0.337	0.484

Copper ground plane circuits with copper inserts are discussed next. Fig. 3.14 shows the transmission response for the family of curves as a function of applied magnetic field for the no insert copper ground circuit. As with the no insert case shown in Fig. 3.12 and 3.13, at 4 GHz the transmission is highest and it drops as the frequency increases.

Figure 3.14: copper ground, no insert, family of curves

Tables 3.4 and 3.5 show all insert cases for their 0 kOe measurements. When the DC B-field is applied the transmission response shifts at the 0 kOe point for some frequencies (usually 6, 10, and 12). This data is useful for showing how the circuits have changed once the inserts have been biased by the magnetic field. The copper inserts are showing significant difference with applied magnetic field, but only at specific frequencies (greater than 10%, 6, 12 and 14 GHz for copper wide insert, 10 and 18 GHz for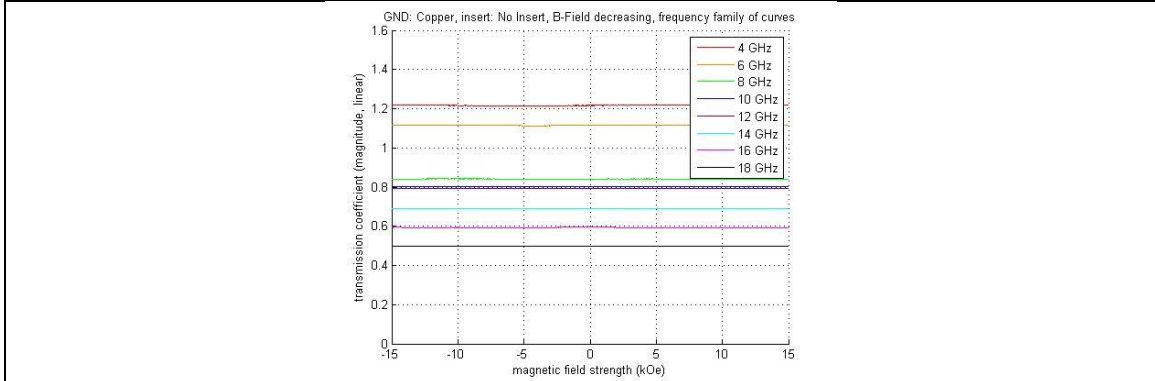 copper narrow, 10, 12, 14, 16, and 18 GHz for the copper square insert). The nickel inserts also strongly change with the application of magnetic field (10, 14, and 18 GHz for nickel wide, 10 and 16 GHz for nickel narrow, and 10 GHz for nickel square).

Table 3.4 Transmission values for all copper inserts and the no insert measurement

F (GHz)	AC B-field / DC + AC B-field			
	No Insert	Copper Wide	Copper Narrow	Copper Square
4	1.179/1.217	1.152/1.162	1.167/1.18	1.149/1.12
6	1.09/1.11	0.424/0.884	0.775/0.817	1.092/1.10
8	0.85/0.842	0.72/0.691	0.728/0.698	0.743/0.805
10	0.817/0.802	0.639/0.676	0.531/0.595	0.308/0.164
12	0.788/0.791	0.635/0.697	0.669/0.666	0.601/0.695
14	0.681/0.69	0.319/0.366	0.535/0.585	0.651/0.505
16	0.578/0.594	0.247/0.236	0.355/0.354	0.533/0.370
18	0.497/0.498	0.229/0.240	0.207/0.174	0.454/0.300

Table 3.5 Transmission values for all nickel inserts and the no insert measurement

F (GHz)	AC B-field / DC + AC B-field			
	No Insert	Nickel Wide	Nickel Narrow	Nickel Square
4	1.179/1.217	1.148/1.16	1.087/1.19	1.18/1.15
6	1.09/1.11	0.68/0.721	0.723/0.746	1.09/1.05
8	0.85/0.842	0.772/0.753	0.756/0.8	0.828/0.817
10	0.817/0.802	0.645/0.372	0.708/0.648	0.799/0.231
12	0.788/0.791	0.643/0.584	0.677/0.644	0.714/0.739
14	0.681/0.69	0.457/0.383	0.592/0.641	0.656/0.610
16	0.578/0.594	0.467/0.437	0.445/.406	0.493/0.456
18	0.497/0.498	0.429/0.358	0.337/.334	0.484/0.442

Figure 3.15 shows the two wide inserts compared against each other. The nickel inserts vary with magnetic field strength at every frequency point measured. At 4, 8, 14, 16, and 18 GHz the transmission increases with the nickel insert when compared to the copper insert while at 6, 10, and 12 GHz the transmission decreases. The nickel measurements are almost symmetrical around their 0 kOe points. At 6 GHz the transmission of the nickel insert begins below that of copper before rising over copper for a 4 kOe window that is symmetric around the 0 kOe point.

(a)   (b)

(c)   (d)
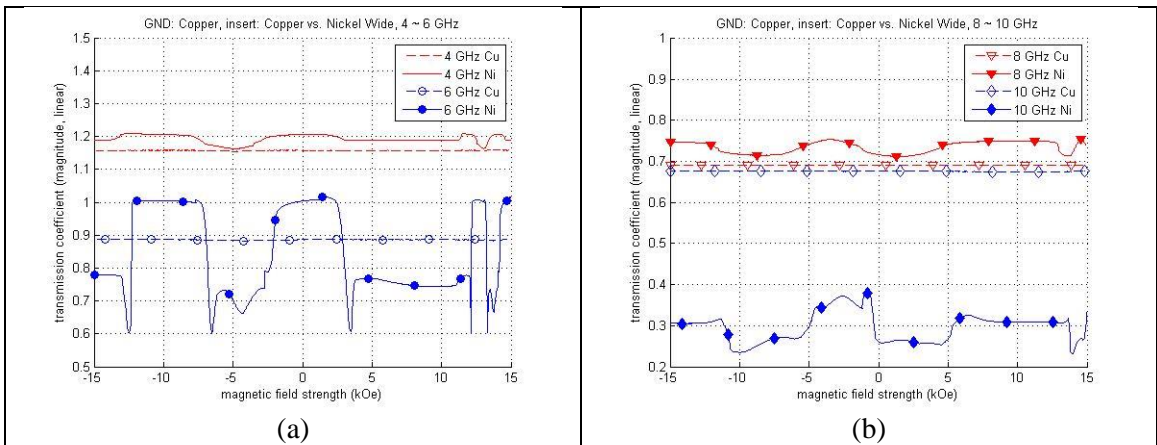
Figure 3.15 A family of curves for the wide inserts grouped into (a) 4 and 6 GHz, (b) 8 and 10 GHz, (c) 12 and 14 GHz, (d) 16 and 18 GHz for a swept B-Field. The copper inserts are dashed lines and hollow symbols. The nickel inserts are solid lines and filled symbols.

Fig. 3.16 shows the two narrow inserts compared against each other. The nickel inserts vary with magnetic field strength at every frequency point measured except for 8 GHz. At 4, 8, 10, 14, 16, and 18 GHz the transmission increases with the nickel insert when compared to the copper insert while at 6, 10, and 12 GHz the transmission decreases. The nickel measurements are almost symmetrical around their 0 kOe points. At 12 GHz the transmission of the nickel insert begins below that of copper before rising over copper for a 4 kOe window that is symmetric around the 0 kOe point.
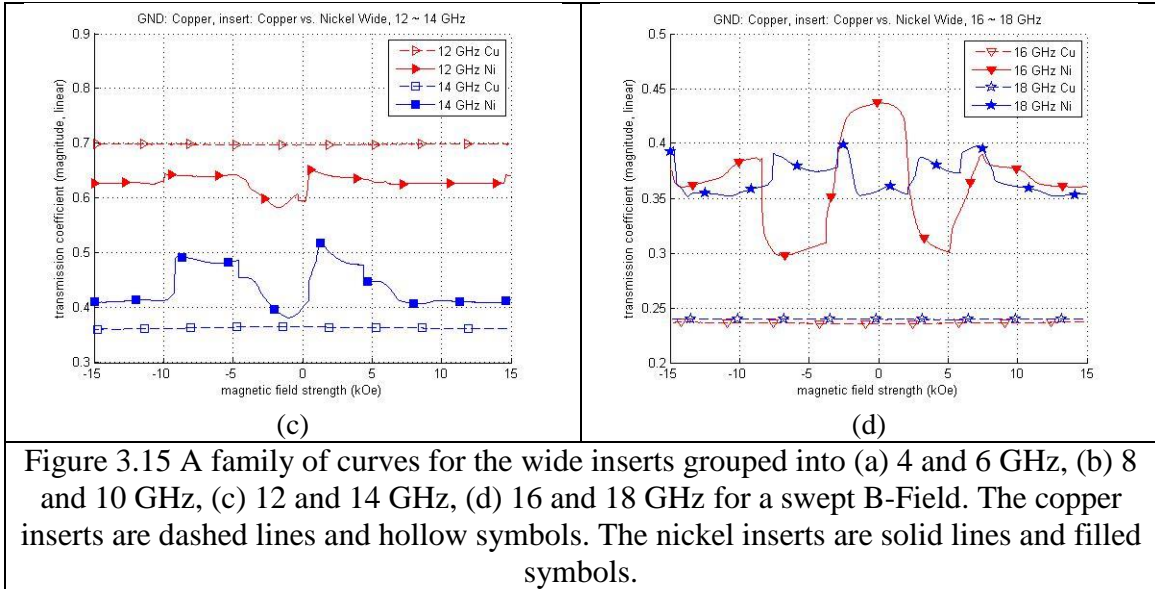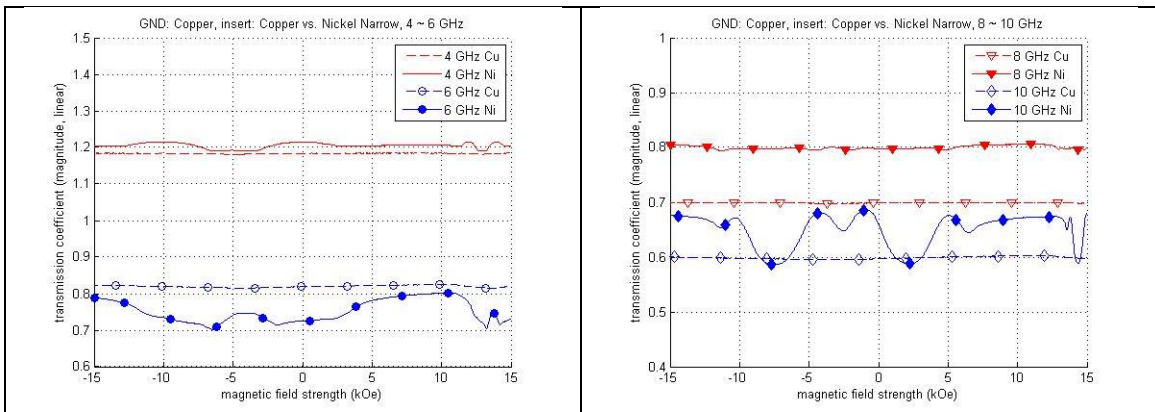
(a)	(b)

(c)	(d)

Figure 3.16 A family of curves for the narrow inserts grouped into (a) 4 and 6 GHz, (b) 8 and 10 GHz, (c) 12 and 14 GHz, (d) 16 and 18 GHz for a swept B-Field. The copper inserts are dashed lines and hollow symbols. The nickel inserts are solid lines and filled symbols.

Fig. 3.17 shows the two square inserts compared against each other. The nickel inserts vary with magnetic field strength at every frequency point measured except for 8 and 12 GHz. At 4, 8, 10, 12, 14, 16, and 18 GHz the transmission increases with the nickel insert when compared to the copper insert while at 6 GHz the transmission decreases. The nickel measurements are almost symmetrical around their 0 kOe points.
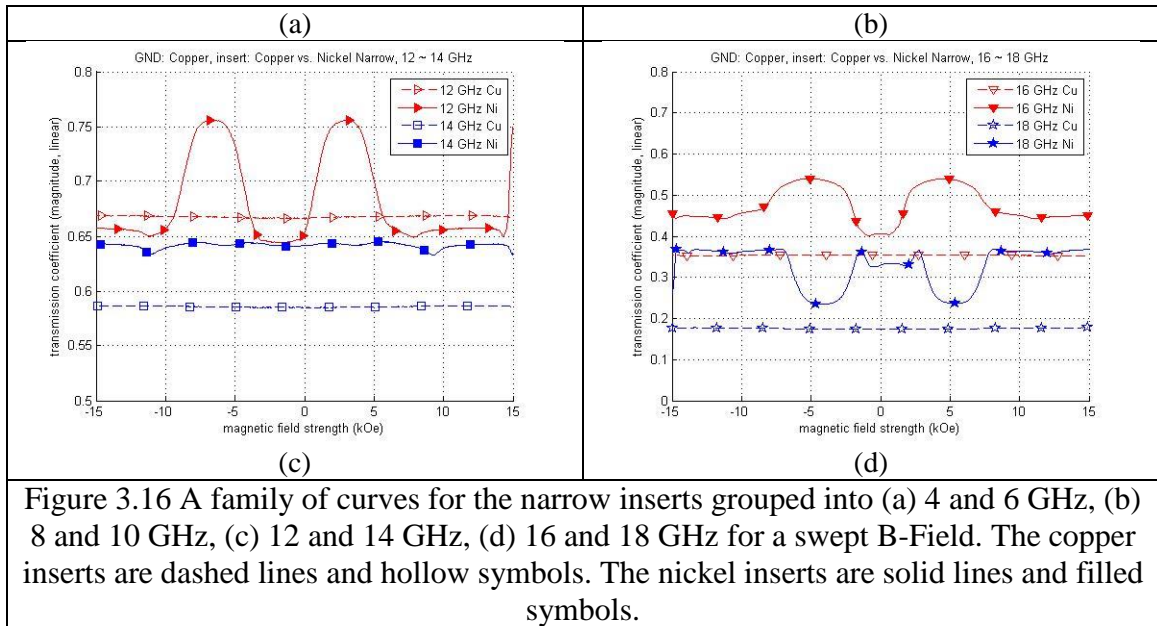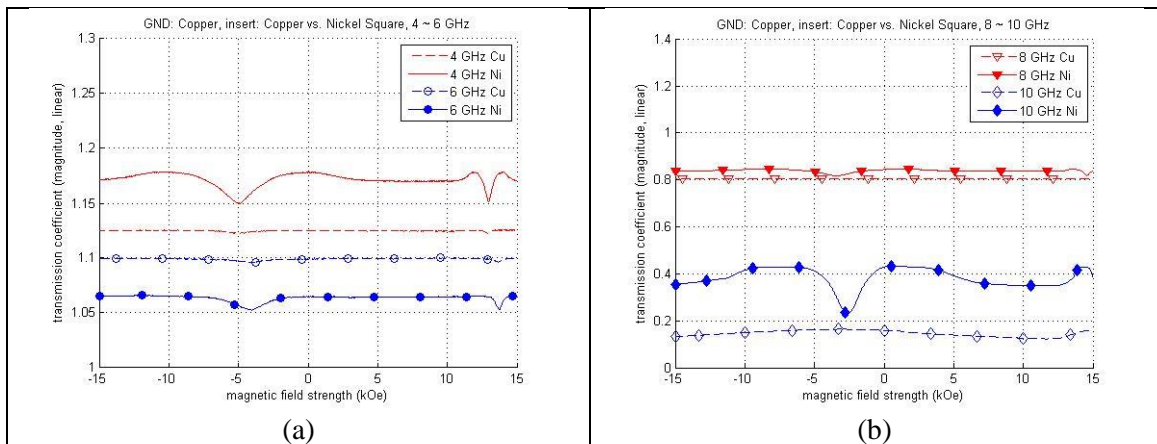

(a)	(b)
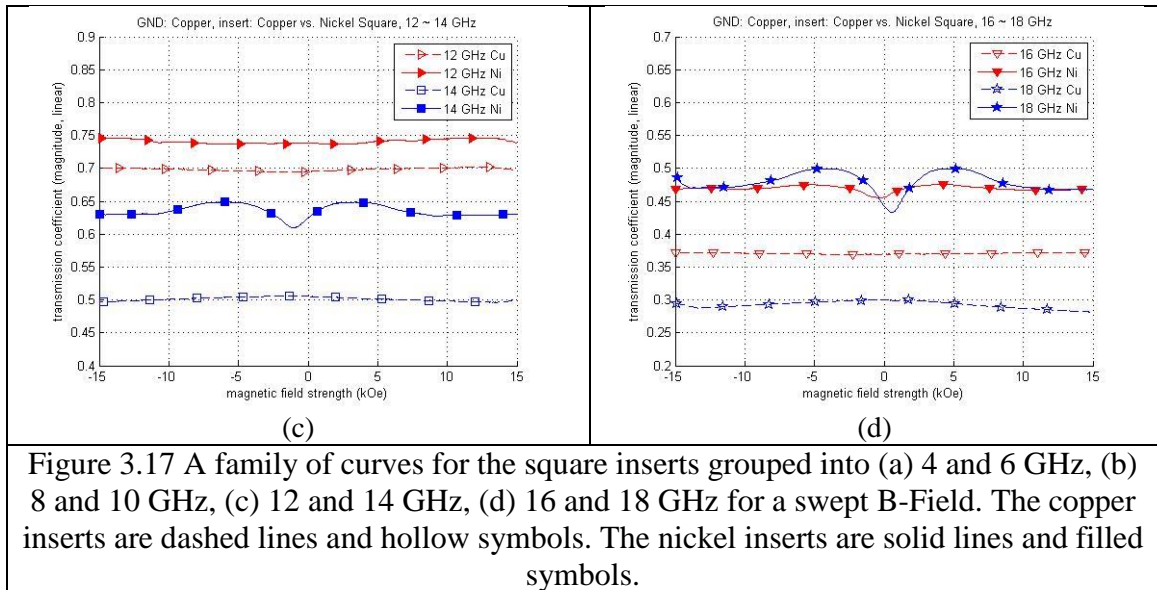
Figure 3.17 A family of curves for the square inserts grouped into (a) 4 and 6 GHz, (b) 8 and 10 GHz, (c) 12 and 14 GHz, (d) 16 and 18 GHz for a swept B-Field. The copper inserts are dashed lines and hollow symbols. The nickel inserts are solid lines and filled symbols.

Overall with the high field measurements it can be shown that while the nonmagnetic insert does not vary with magnetic field strength, the magnetic nickel inserts vary with applied DC B-field.

3.6   Conclusion

In this chapter microstrip lines were evaluated with a strong DC magnetic field applied to test if magnetic material response would change over the frequency sweep. The nonmagnetic copper inserts did not change with applied magnetic field, but the magnetic nickel inserts experienced changes with magnetic field strength. The wide and narrow nickel inserts displayed a change in transmission between -7.5 kOe and 7.5 kOe where around 0 kOe there was no change and as the field strengthened in either direction the transmission increased or decreased before returning to a flat line outside of that

range. Even though the nanowire sample could not be placed inside the microstrip line as

the other inserts before it, it was tested but no FMR was observed.

Chapter 4

Conclusion and future work

4.1 Summary and Conclusions

Chapter 2 characterized a microstrip test structure with varied ground planes and with varied inserts with AC magnetic fields applied as a part of RF signals. Chapter 3 characterized similar microstrip test structures inside DC magnetic fields to test the reaction of magnetic materials to RF signals while saturated by a DC field. With no DC magnetic field changing the ground plane does not appreciably change the response of the microstrip line, and also adding inserts changes the response by adding another propagation mode to the transmission. Full wave simulation tools, such as HFSS, are the best at simulating these bulk magnetic materials but overall their response cannot be predicted by computer models. When DC magnetic fields are added the circuits with nonmagnetic inserts do not appreciably change, but the magnetic inserts display a change in transmission at specific frequencies as the magnetic field is swept.

4.2 Future work

This work shows that there is some variation in bulk magnetic material response to DC magnetic field. Only one magnetic material was tested in this work; many magnetic materials could be tested and a reference of their responses could be characterized. Nanowires could not be measured in the same way that the magnetic inserts were. It would be nice for the test structure that fits in the Electromagnet to be

able to test nanowires inside the substrate where they can be excited by a strong electric and magnetic field simultaneously. The test structure would be better if it could be two layers of FR4 dielectric with no air gap, so the insert is completely surrounded in FR4, or with the insert able to be placed at different distances from the signal line and ground plane in the test circuit to determine how response changes with circuit structure. Finally, being able to synchronize the DC magnetic field measurements without drift between frequencies would be allow more confidence in determining whether changes in response are due to the DC magnetic field bias.

Bibliography

[1] N. Bloembergen "On the Ferromagnetic Resonance in Nickel and Supermalloy" in Physical Review, volume 78, number 5, 572-580, June 1950

[2] M. Sharma, S. Pathak, M. Sharma, "FMR Measurements of Magnetic Nanostructures," *Intech Open*, July 31st, 2013. [online] Available: https://www.intechopen.com/books/ferromagnetic-resonance-theory-and-applications/fmr-measurements-of-magnetic-nanostructures . [Accessed: Dec. 18, 2017]

[3] K J Standley and K H Reich. "Ferromagnetic Resonance in Nickel and in some of its Alloys" in *Proc. Phys. Soc. B*, vol. 68, no. 10, pp 713-722, May 1955

[4] J. Lee and Y. Hong. "Ferrites for RF Passive Devices", *Solid State Physics*, Vol. 64, pp 237-329, 2013

[5] M. Sharma, B. K. Kumar, M. Sharma, A. Basu. "Tunable Coplanar Waveguide Microwave Devices on Ferromagnetic Nanowires," in *Conference: 2013 4th International Conference on Nano Science and Technology ICNST, Sept. 16, 2013, New Delhi, India* [Online]. Available: researchgate, https://www.researchgate.net. [Accessed: Dec. 18, 2017]

[6] L. Yuan, S. Meng, Y. Shi, Y. Zhang, Z. Yue, and L. Li. "Dual band microwave ferromagnetic resonance absorption in annealed cobalt nanowire arrays" *Applied Physics Letters*, vol. 105, issue 18, pp 182407 1-3.

[7] R.Ramirez-Villegas, I. Huynen, L. Piraux, A. Encinas, J. De La Torre Medina "Configurable Microwave Filter for Signal Processing Based on Arrays of Bistable Magnetic Nanowires," *IEEE Transactions on Microwave Theory and Techniques*, vol 65, no 1, 99. 72-77, Jan 2017

[8] Y. Li, L. Li, J. Cai. "Dual-Band Noise Suppressors Based on Co/Au Multilayered Magnetic Nanowires". IEEE Transactions on Magnetics, vol 48, no 11, pp 4398-4401, Nov 2012.

[9] A. Saib, M. Darques, L. Piraux, D. Vanhoenacker-Janvier, I. Huynen. "Unbiased microwave circulator based on ferromagnetic nanowires arrays of tunable magnetization state," Journal of Physics D: Applied Physics, vol 38, no 16, pp. 2759-2763, Aug. 2005

[10] G. Hamoir, L. Piraux, I. Huynen. "Control of Microwave Circulation Using Unbiased ferromagnetic Nanowires Arrays" IEEE Transactions on Magnetics, vol 49, no 7, 4261-4264, July 2003.

[11] V. V. Risser Jr., "Design and construction of microstrip circulators" (1969). [Online] Available: http://lib.dr.iastate.edu/rtd/4683 [Accessed Dec 18, 2017]

[12] I. Harward, T. O'Keevan, A. Hutchison, V. Zagorodnii, and Z. Celinski. "A Broadband Ferromagnetic Resonance Spectrometer to Measure Thin Films Up to 70 GHz". *Review of Scientific Instruments*, vol. 82, issue 9, pp. 095115 1-7.

[13] M. Sharma, B. Kuanr, M. Sharma, A. Basu "New Opportunities in Microwave Electronics with Ferromagnetic Nanowires," Journal of Applied Physics, vol 115, no 17A518, pp1-3, Feb. 2014.

[14] J. Spiegel, L. Piraux, I. Huynen. "Ferromagnetic Material with Negative Permeability for Tunable Left-handed Devices". *Proceedings of the 37th European Microwave Conference*, Oct, 2007, Munich Germany.

[15] S. S. Kalarickal, P. Krivosik, M. Wu, C. E. Patton. "Ferromagnetic resonance linewidth in metallic thin films: Comparison of measurement methods," Journal of Applied Physics, vol 99, no 093909, pp. 1-7, May. 2006

[16] I. S. Maksymov, M. Kostylev "Broadband Stripline Ferromagnetic Resonance Spectroscopy of Ferromagnetic Films, Multilayers and Nanostructures" *Physica E: Low-dimensional Systems and Nanowstructures*, vol. 69, pp 252-293, May 2015.

[17] C. Bilzer, T. Devolder, P. Crozat, C. Chappert, S. Cardoso, P. P. Freitas. "Vector Network Analyzer Ferromagnetic Resonance of Thin Films on Coplanar Waveguides: Comparison of Different Evaluation Methods". Journal of Applied Physics, vol 101, no 074505, pp. 1-5, 2007

[18] Y. Endo, Y. Shimata, M. Yamaguchi. "Study on the Magnetization Dynamics of Ni–Fe Dot Arrays Estimated by the CPW-FMR Measurement Method," IEEE Transactions on Magnetics, vol 51, no 11, 3517-3519, Nov. 2015

[19] "S. Sievers, J. Kurda, N. Liebing, F. Hohls, and H. W. Schumacher. "Microwave Inferometry for High Sensitivity VNA-FMR Measurements," IEEE Transactions on Magnetics, vol. 53, no. 4, Apl 2017.

[20] V. Bhat, J. Woods, J. T. Hastings, L. E. De Long, J. Sklenar, J. B. Ketterson, O. Heinonen, K. Rivkin, V. Metlushko. "Low-Field FMR Studies of Magnetic Confinement Effects in Patterned Ferromagnetic Thin Films" *IEEE Transactions on Magnetics*, vol. 42, no. 10, pp 3225-3227, Oct 2006.

[21] H. Koizumi, M. Sato, Y. Ando, S. Ishio, and T. Miyazaki. "FMR Study of Ni-Fe/Cu Multilayer Films," IEEE Translation Journal on Magnetics in Japan, vol 9, no 6, 242-246, Nov 1994.

[22] I. Dumitru, F. Li, J. B. Wiley, D. Cimpoesu, A. Stancu, and L. Spinu. "Interaction Effects Analysis of Fmr Spectra on Dense Nanowire Systems," IEEE Transactions on Magnetics, vol. 42, no. 10, Oct 2006.

[23] A. Encinas-Oropesa, M. Demand, and L. Piraux. "Dipolar Interactions in Arrays of Nickel Nanowires Studied by Ferromagnetic Resonane," Physical Review B, vol. 63, no 104415, pp. 1-6, Feb 2001.

[24] L. Yuan, Z. Yue, S. Meng, and L. Li "High-Frequency Ferromagnetic Resonance of Co Nanowire Arrays," Phys. Status Solidi A, vol. 211, no. 8, pp. 1828-1833, Apl. 2014

[25] A. S. Sokolov, M. Geiler, V. G. Harris. "Broadband ferromagnetic resonance linewidth measurement by a Microstripline transmission resonator," Journal of Applied Physics Letters, vol 108, issue 17, pp. , Apl. 2016

[26] U. Ebels, J. -L. Duvail, P. E. Wigen, L. Piraux, L. D. Buda, and K. Ounadjela. "Ferromagnetic resonance studies of Ni nanowire arrays," Phys. Rev. B, vol 64, no 144421, pp. 1-6, Sep. 2001

[27] D. M. Pozar, *Microwave Engineering,* Fourth Edition, Hoboken, NJ: Wiley, Nov. 2011.

[28] *Advanced Design System, 2015.1*. Santa Rosa, Ca: Keysight Technologies Inc., 2014.

[29] "Isola 185 HR," 2016. [Online] Available: http://www.isola-group.com. [Accessed: Jan. 19, 2017]

[30] "Du Pont Teijin Films Melinex 462," 2006. [Online] Available: http://69.67.54.76/FilmEnterprise/Datasheet.asp?Result=Print&ID=697&Version=US. [Accessed: Jan. 19, 2017]

[31] I. Dumitru, L. Spinu, F. Li, J. B. Wiley, D. Cimpoesu, A. Stancu. "Interaction effects analysis of dense nanowire systems FMR spectrum" in *2006 IEEE International Magnetics Conference (INTERMAG), May 8, 2015, San Diego, CA, USA* [Online]. Available: IEEE Explore, http://ieeexplore.ieee.org. [Accessed: Dec 18, 2017]

[32] *HFSS Version 15.0.* Canonsburg, PA: ANSYS, Inc. 1970.

[33] *Q3D Extractor Version 10.0*. Canonsburg, PA: ANSYS, Inc. 1970.

[34] "Universal Substrate Test Fixture," 2008. [Online] Available: http://www.icmicrowave.com [Accessed: Jan. 19, 2017]

[35] *Origin 9*. Northhampton, MA: OriginLab Corp, 1992

[36] Milling Machine ProtoMat S103, LPKF, Inc, Wilsonville, OR, 1976.

[37] "Lightning 37000D Vector Network Analyzers" [Online] Available: https://dl.cdn-anritsu.com/en-us/test-measurement/files/Brochures-Datasheets-Catalogs/Brochure/11410-00346.pdf [Accessed Dec 18, 2017

[38] "Understanding VNA Calibration" [Online] Available: http://anlage.umd.edu/Anritsu_understanding-vna-calibration.pdf [Accessed Dec 18, 2017]

[39] *WinCal, Version 3.2.0.* Beaverton, OR: Cascade Microtech, 2001.

[40] "SMA 50 Ohm End Launch Jack Receptacle – Round contact," 2010. [Online] Available: https://belfuse.com. [Accessed: Jan 19. 2017]

[41] W. Zhou, "Nelson_2017_11_13_VSMAnalysisCode_3.m", unpublished

[42] *MATLAB, R2011a*. Natick, MA: Mathworks Corporation, 2004.

APPENDIX A

VNA Block Diagram

Fig. A.1 shows the VNA measurement setup used in chapter 2. Fig A.2 shows the VNA measurement setup used in chapter 3. The cables and connectors that link the VNA to the microstrip (DUT) are included.

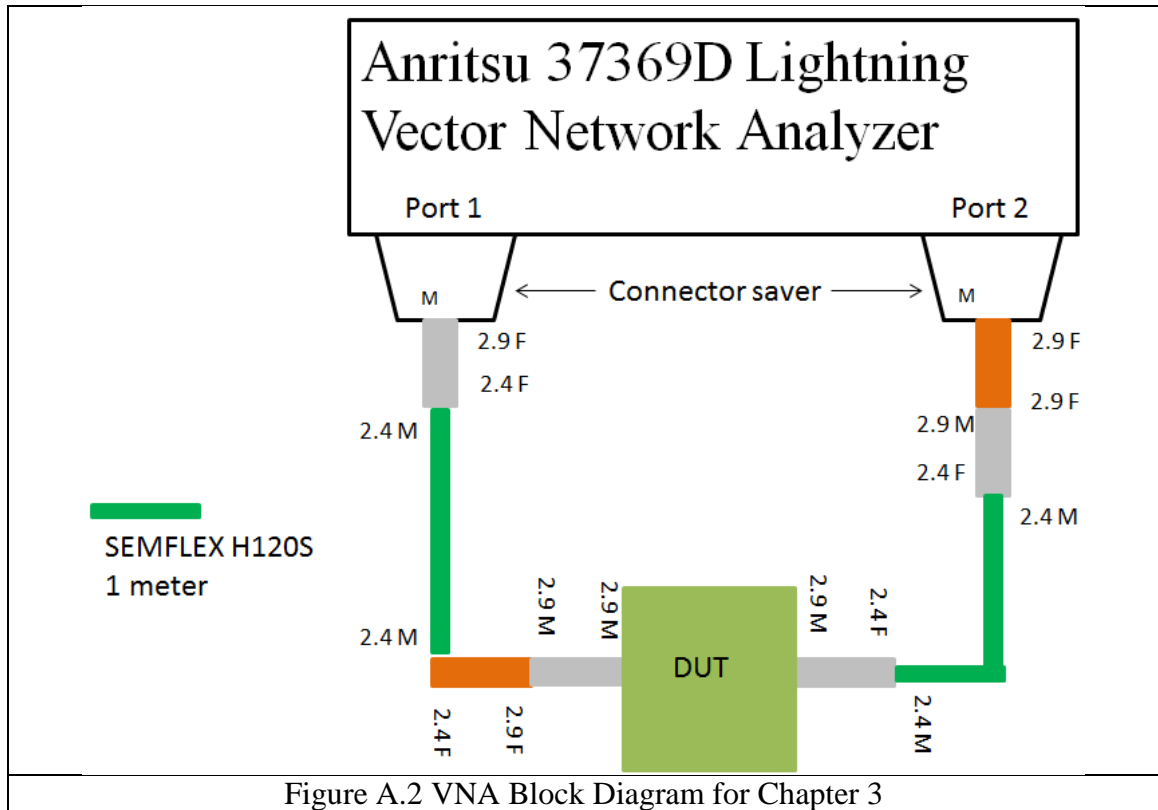Figure A.1 VNA Block Diagram for Chapter 2
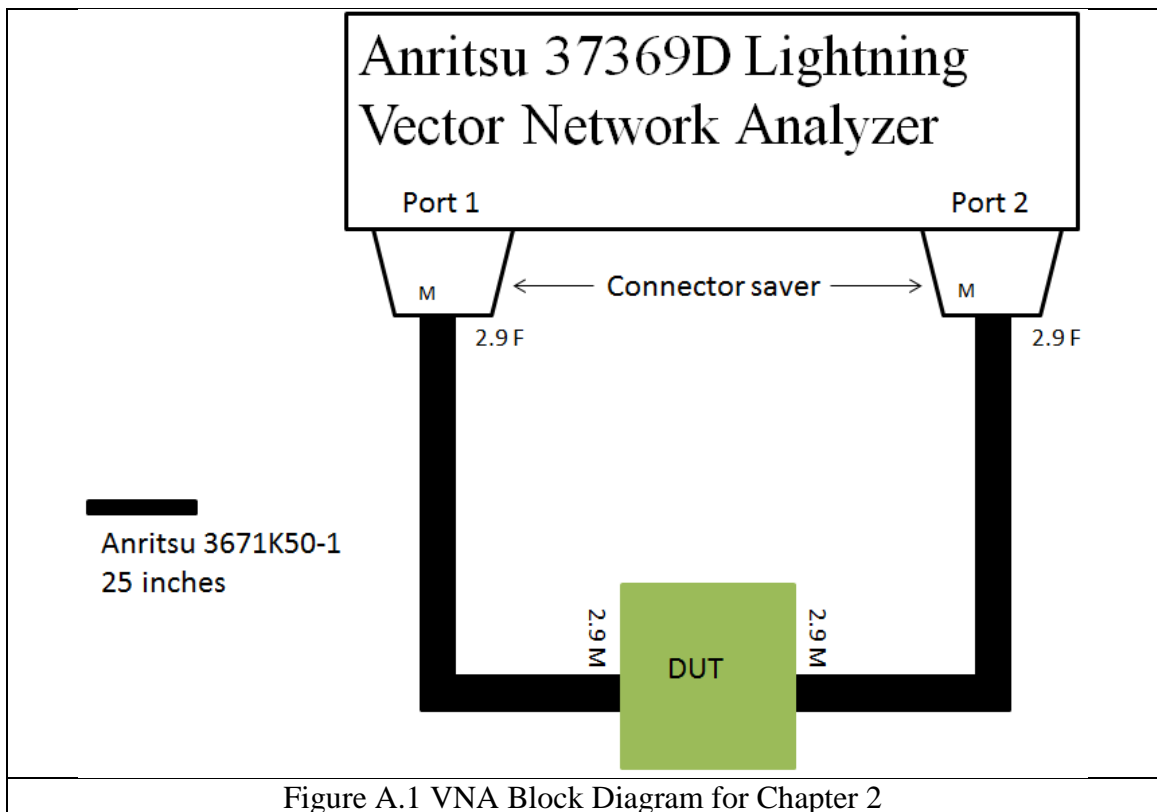
Figure A.2 VNA Block Diagram for Chapter 3

Fig. A.3 shows the connector of the UTF connected to the microstrip line with its dimensions defined in Table A.1. Fig. A.4 show the SMA connection to the microstrip line with its dimensions defined in Table A.2. The dimensions in Tables A.1 and A.2 are outer diameter of the coaxial connector (Do), inner diameter of the coaxial connector (Di), signal line thickness (tc), FR4 dielectric thickness (h), insert thickness (ti), Melinex thickness (tp), and thickness of the ground plane (tg). The size of the outer diameter of the coaxial line needs to reach the ground plane of the microstrip line in order to properly transfer the fields from the coaxial mode to the microstrip mode, but the UTFs Do is too small for this. The decrease in transmission of the UTF lines below 3 GHz maybe related to this structural oversight.

Table A.1 dimensions of microstrip line used in chapter 2

Dimension	Do	Di	tc	h	ti	tp	tg
mils	59.1	18.5	1.4	28	1.4 (cu) or 3 (ni)	2	1.4 (cu) or 6 (ni)

Table A.2 dimensions of microstrip line used in chapter 3

Dimension	Do	Di	tc	h	ti	tp	tg
mils	150	35	1.4	28	1.4 (cu) or 3 (ni)	2	1.4

Figure A.3 UTF connection to microstrip

Figure A.4 SMA connection to microstrip
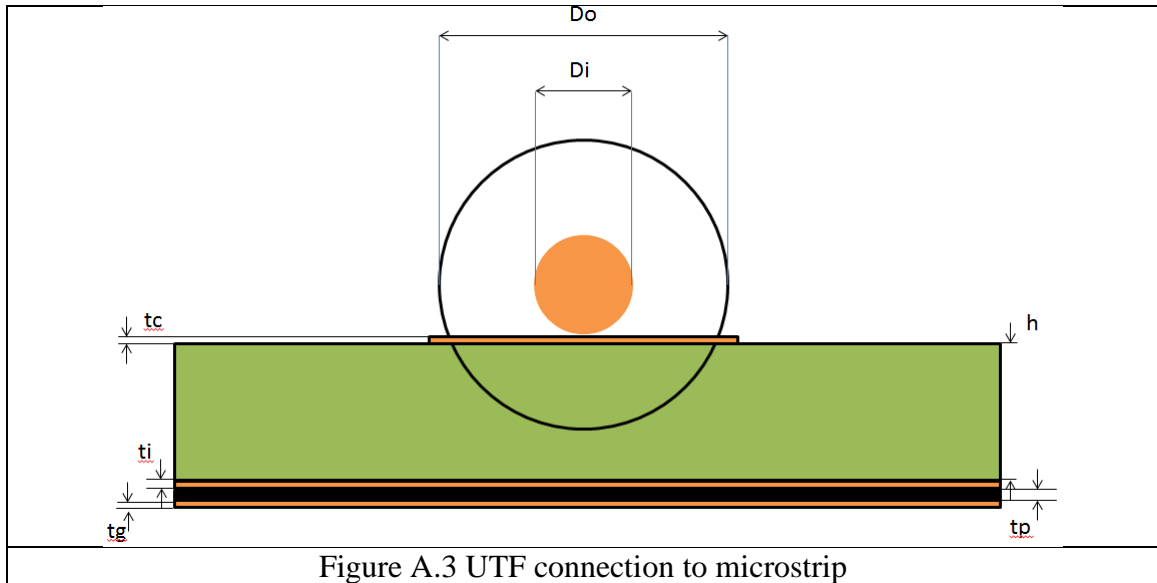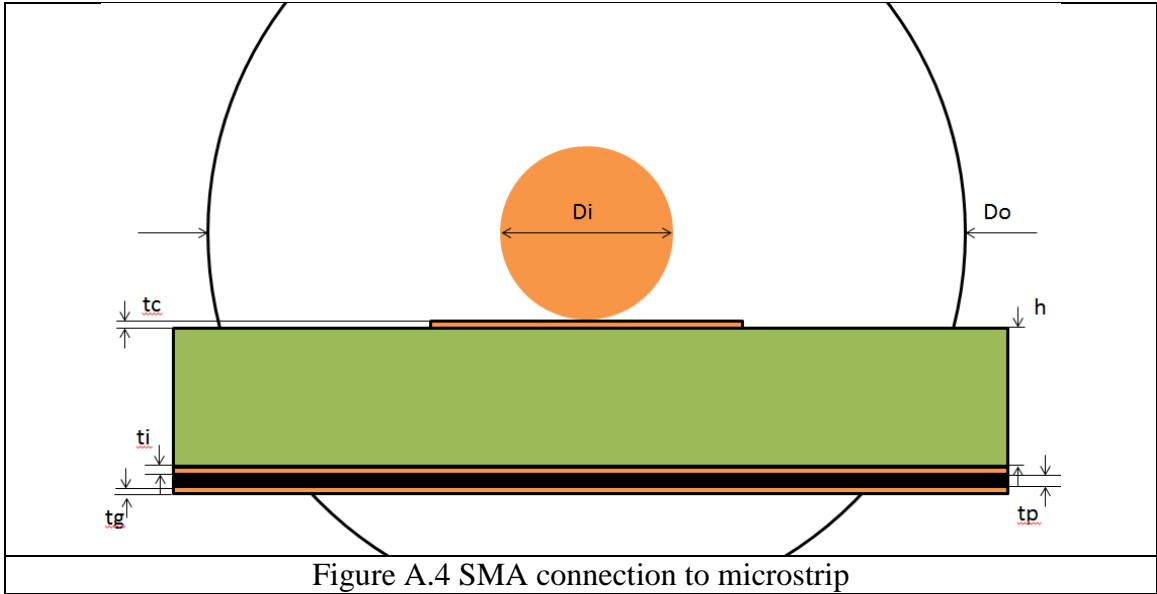
Appendix B

ADS Equivalent Circuit models

Chapter 2 measured microstrip lines with magnetic and non-magnetic inserts; this chapter will model the microstrip lines by modeling their impedances in ADS. The nickel and copper inserts change the impedance of the microstrip transmission lines by adding a parallel plate interaction between themselves and the ground plane and signal line and creating an air gap between the two dielectric layers. To illustrate these two sections: Figs. B.1a and B.1b show a cross section of an HFSS simulation with cuts through it for the 2 domains to demonstrate the two sections that Q3D impedance measurements are run for: with insert, and feedline (without insert). Fig. B.1a shows the simulation regions for a square insert and Fig. B.1b shows the simulation regions for a narrow insert. Both domains are simulated through Q3D to find the impedance of the line, and the impedances are plugged into ADS as shown in Fig. B.1c for the square insert.

The ADS simulation is different from the original ADS simulation in chapter 2 to account for the microstrip line no longer behaving like an ideal structure. The TLINP simulation is used in place of the standard microstrip because the impedance from Q3D can be assigned to the specific frequency. The most important reason to switch to TLINP is that conductor attenuation (A, dB/meter) can be defined directly for both the nickel and copper cases with numbers calculated through Eqns 5 & 6 from chapter 2. When Eqns 5 & 6 are solved for copper and nickel the conductor attenuation is $A_{cu} = 5.95 \times 10^{-7}$ dB/meter and $A_{ni} = 1.22 \times 10^{-7}$ dB/meter respectively. There are coaxial transmission

lines on both ends of the model to simulate the ends of the fixture. Table B.1 below lists the impedances from the Q3D simulations in the two sections simulated for copper ground circuits.
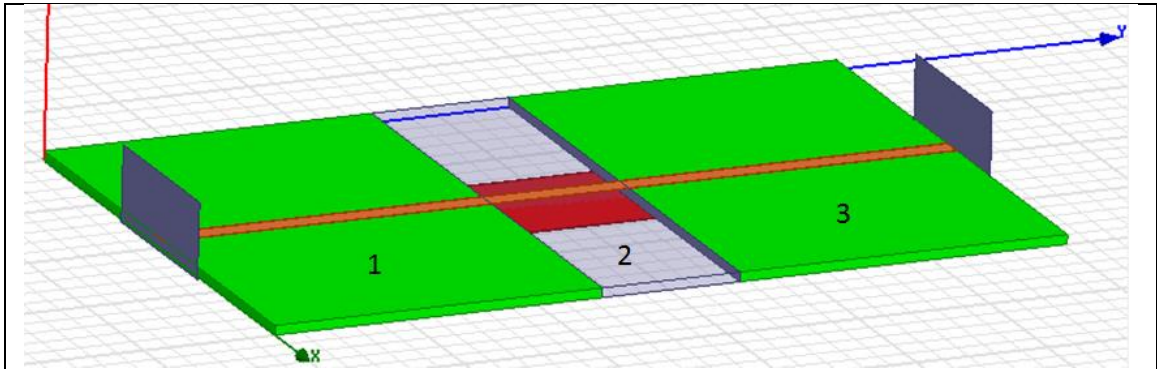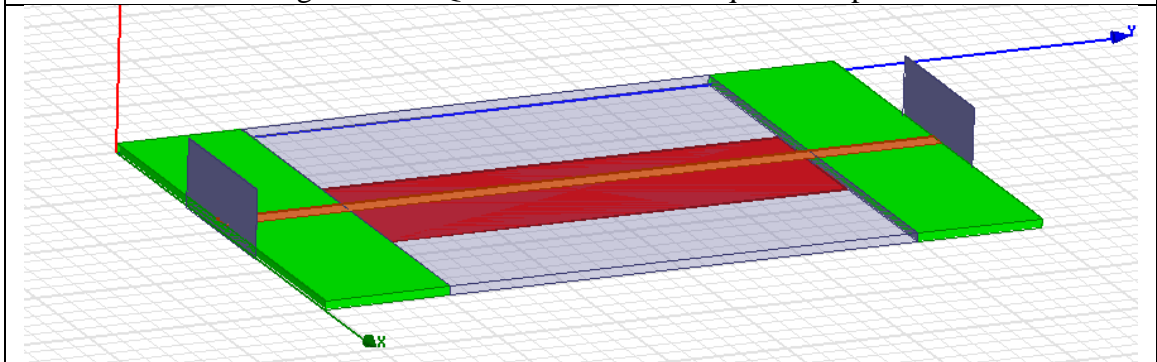

Figure B.1a: Q3D simulation of a square sample

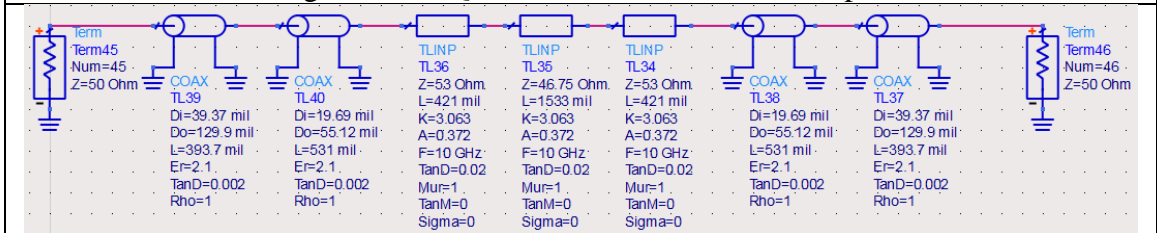Figure B.1b: Q3D simulation of narrow sample

Figure B.1c: ADS simulation built from Q3D simulations

Table B.1: Impedances of Copper Ground circuits

Circuit	Sections 1 & 3 Impedance	Section 2 Impedance
No Sample	49.6	49.6
Copper Wide	53	46.75
Copper Narrow	53	47.25
Copper Square	53	47.48
Nickel Wide	56.05	46.83
Nickel Narrow	56.05	47.23
Nickel Square	56.05	47.32

The no insert with copper ground and copper wide with copper ground measurements will be compared to the ADS models in this chapter. Fig. B.2 shows the no insert ADS simulation (red, solid) compared against the VNA measurement (black, dashed). This model is more similar to the reflection response of the measurement while only being -0.5 dB below the transmission over the entire band. The model's reflection response has a strong periodicity that is similar to the measurement's, but that periodicity breaks down between 7 and 9 GHz and 14.5 and 16 GHz. The model has a longer 8 GHz pattern of higher mismatch for 6 GHz then a stable linear 2 GHz region.

Figure B.2: Reflection (a) and Transmission (b) response for ADS simulation (red, solid) vs VNA Measurement (black, dashed) of the no insert on copper ground
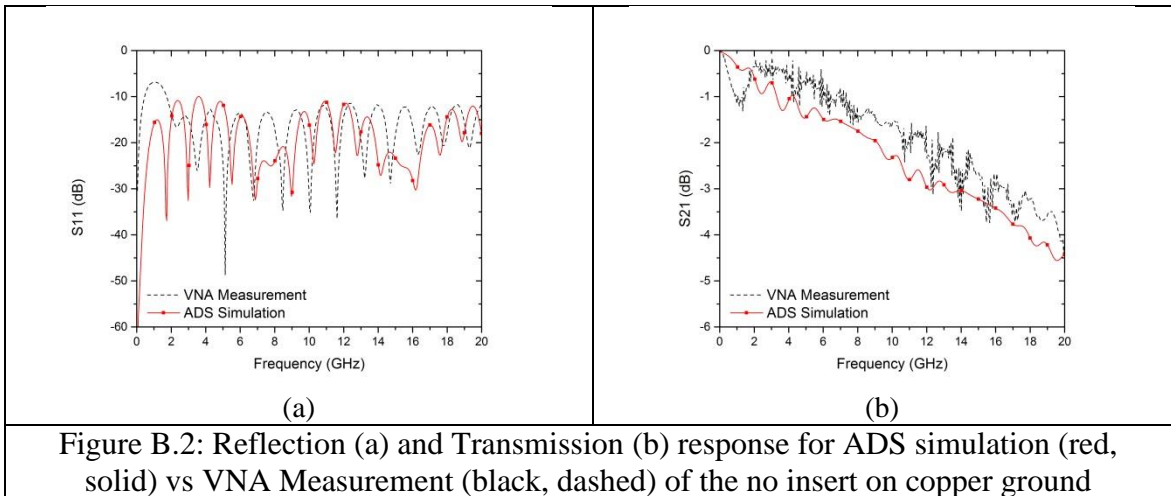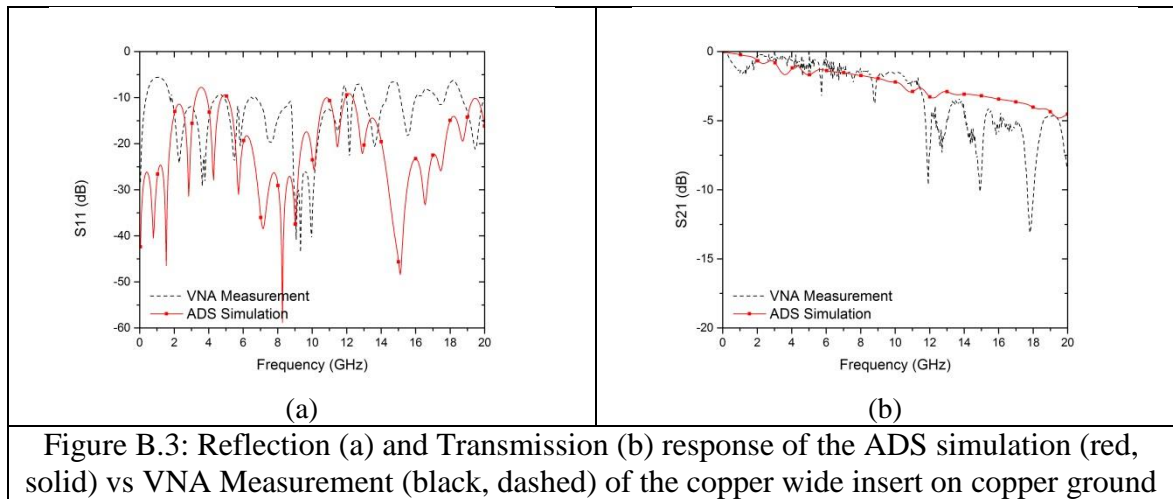
Fig. B.3 compares an ADS circuit model with a wide copper insert and a VNA measurement from section 3.5. The wide insert's ADS simulation matches the VNA measurement's reflection response between 2 and 5 GHz and 9 and 13 GHz, but the model has a 7 GHz pattern of 2 GHz of lower reflection before rising for 3 GHz and then slowly declining for 2 GHz. The transmission response of the model predicts the transmission to be -0.5 dB lower than it is in the measurement, but it captures neither the drop in transmission that occurs at 11.7 GHz nor the nulls at 6 and 9 GHz.

(a)   (b)

Figure B.3: Reflection (a) and Transmission (b) response of the ADS simulation (red, solid) vs VNA Measurement (black, dashed) of the copper wide insert on copper ground
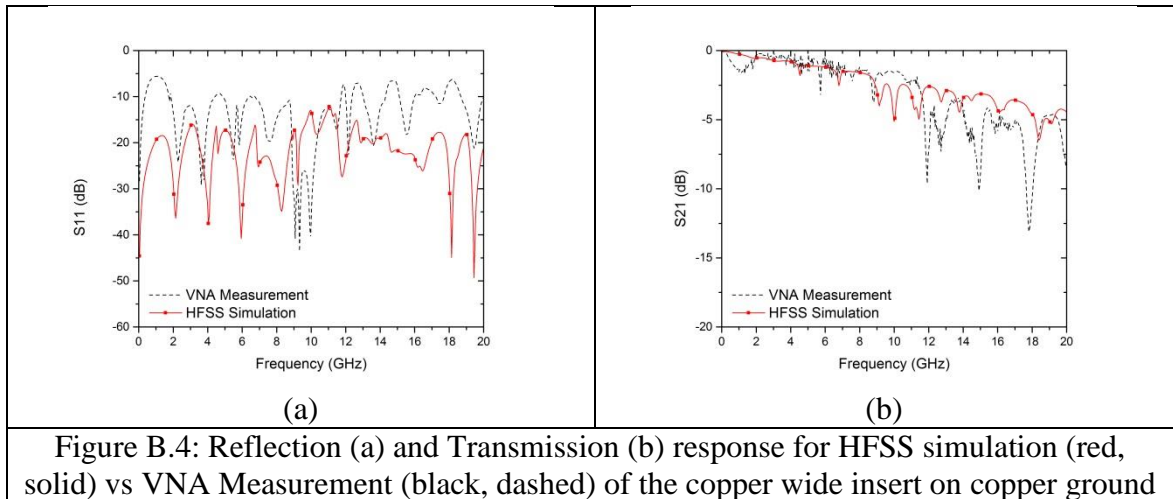
The ADS models are good for predicting the reflection response of the measurements, but the transmission response models a -0.5 dB deviation from the expected transmission response at best while not catching any of the nulls that occur at periodic frequencies. Overall ADS models cannot predict the reflection or transmission responses, only approximating the maximum reflection response and the trendline of the transmission response. The microstrip lines with no insert can be modeled far better than

a microstrip line with an insert, and thus ADS is not useful for determining circuit performance of inserts.

HFSS insert models

In this chapter the HFSS simulations are compared against their measurements on the VNA. The HFSS models were built off the 2 models seen in Chapter 2. All HFSS models presented in this chapter use the same frequency sweeps and excitations as the previous models and the VNA Measurements. The copper wide insert with copper ground plane model will be compared against the VNA measurement from chapter 2. The inserts are placed in between the non-conducting FR4 dielectric substrate and the non-conducting plastic layer. An air gap is between the plastic and FR4 in the space not occupied by the insert. HFSS's meshes cannot converge when the nickel ground is 6 mils thick, so instead the nickel ground planes are 3 mils thick.

In Fig. B.4 the wide copper insert on copper ground HFSS model (red, solid) is compared against the equivalent VNA measurement (black, dashed) from chapter 2. The simulation presents a better reflection below 8.5 GHz and above 11.3 GHz and a similar transmission between 2 and 9 GHz. The transmission of the model dips below that of the measurement between 9 and 11.8 GHz. The resonances at 4.5, 7, 11.5, 14, 16 and 18.2 GHz roughly correspond to the measurement's 3 GHz resonances.

Figure B.4: Reflection (a) and Transmission (b) response for HFSS simulation (red, solid) vs VNA Measurement (black, dashed) of the copper wide insert on copper ground

The HFSS simulations are limitedly useful for predicting the behavior of circuits measured in a VNA. The copper ground plane models are useful above 2 GHz and up to a frequency dependent on the individual insert. The HFSS simulations always predict a superior match than the VNA delivers, but it predicts similar behavior of the transmission response. The HFSS models are not able to capture the dips in transmission that are seen in the VNA measurements, frequently predicting them at different frequencies and with a different periodicity. Ultimately HFSS cannot replicate the VNA Measurements and predict how inserts will behave when inserted into microstrip lines.